Multi-scale imaging/monitoring of fault zone regions and detection of small events

Yehuda Ben-Zion, University of Southern California, with
F. Vernon, A. Allam, P. Share, H. Qiu, L. Qin, F.-C. Lin, G. Hillers, P. Roux, M. Campillo, F. Niu & others

Complex structures with

Hierarchical damage zones

Strong geometrical and material heterogeneities (bimaterial interfaces, distributed damage, fluids, ...)

Strong attenuation and anisotropy

Ongoing and episodic temporal changes of properties

Other challenging ingredients (multi-scale/signal seismic wavefield)

Outline

Use seismic data from the San Jacinto and North Anatolian faults to

1. Image fault zone structures

2. Monitor temporal changes

3. Detect small earthquakes

Results relevant for

- Developing accurate seismic catalogs and analysis of earthquake source properties.
- Evolutionary processes on long (tectonic) and short (e.g., precursory) timescales.
- Static/dynamic stress fields (e.g. from internal fault zone structure).
- Brittle rock rheology (e.g. from observing & monitoring rock damage).
- FZs control crustal fluid flow: hydrology, oil, sub-surface storage, etc.
- Elements of FZ structure (bimaterial interfaces and damage zones) can control future (and reflect past) earthquake rupture properties.

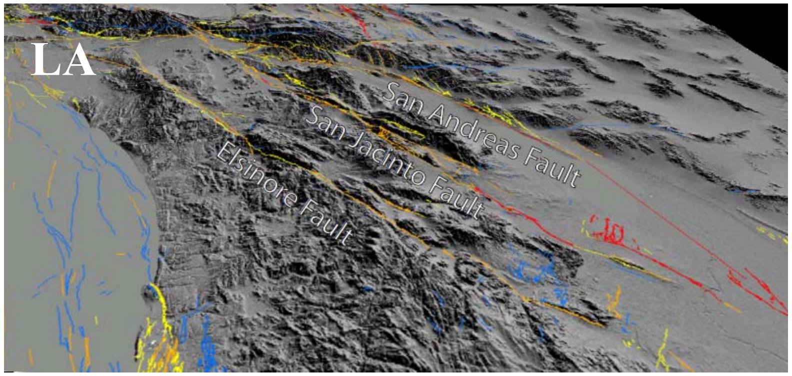

Hierarchical Seismic Networks around the San Jacinto Fault Zone in southern CA

Data: Earthquake waveforms, ambient seismic noise (+ small "Besty" gunshots)

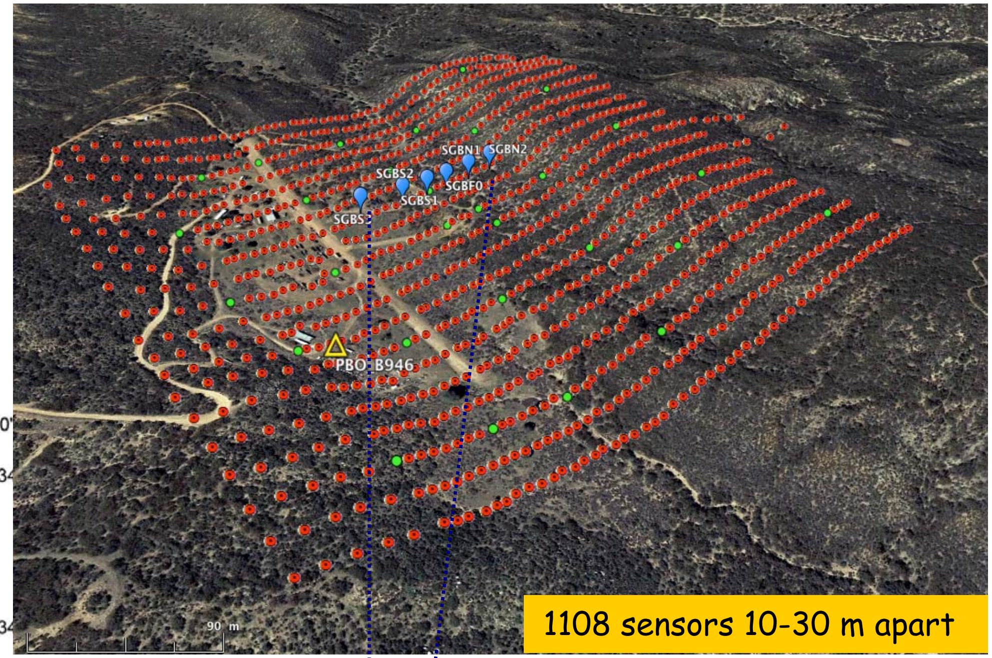

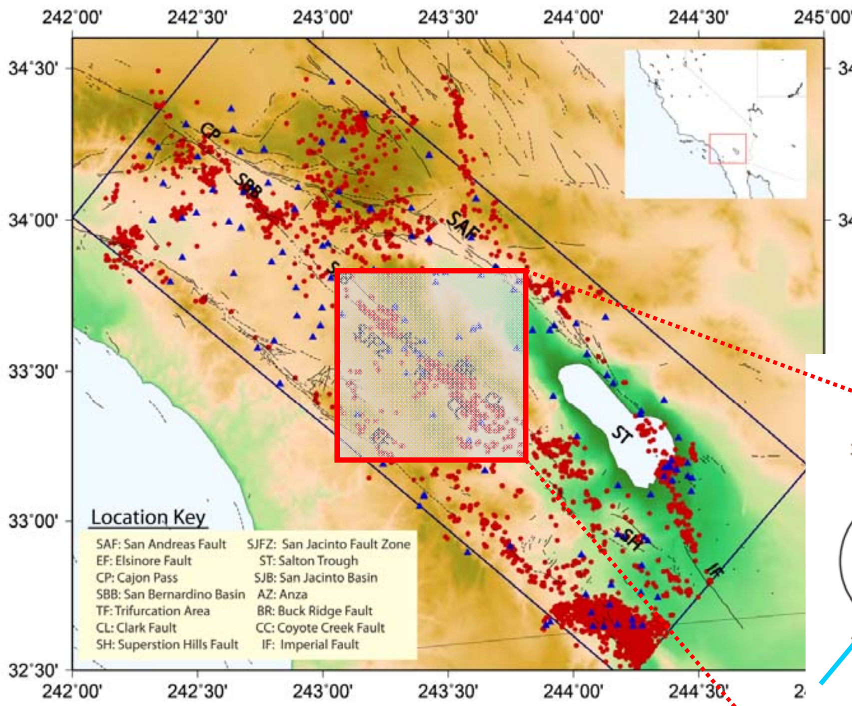

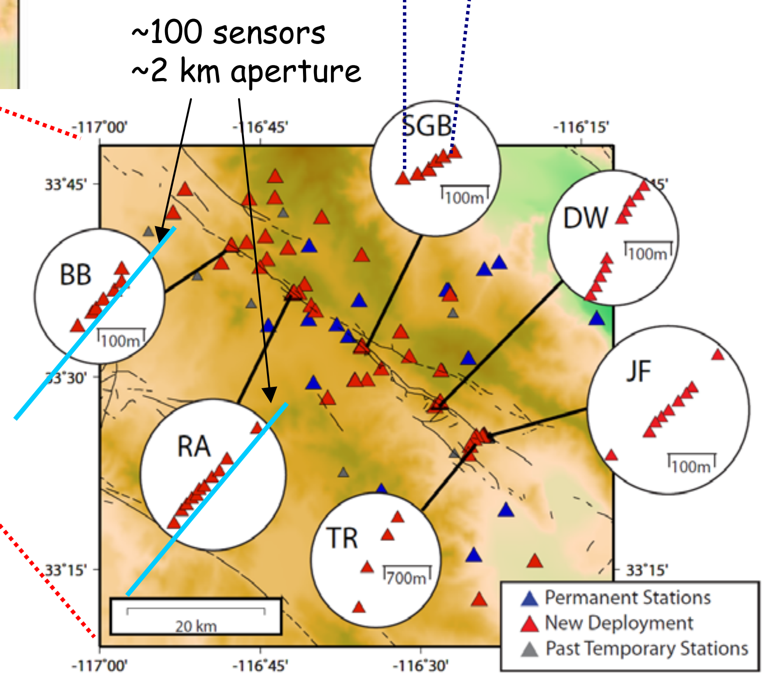

Signals: P & S body waves, Rayleigh & Love surface waves,
Fault zone head & trapped waves
(+ anisotropy and attenuation)

Seismic Velocity Structures in the Southern California Plate Boundary Environment from Double-Difference Earthquake Tomography (Allam and Ben-Zion, GJI, 2012)

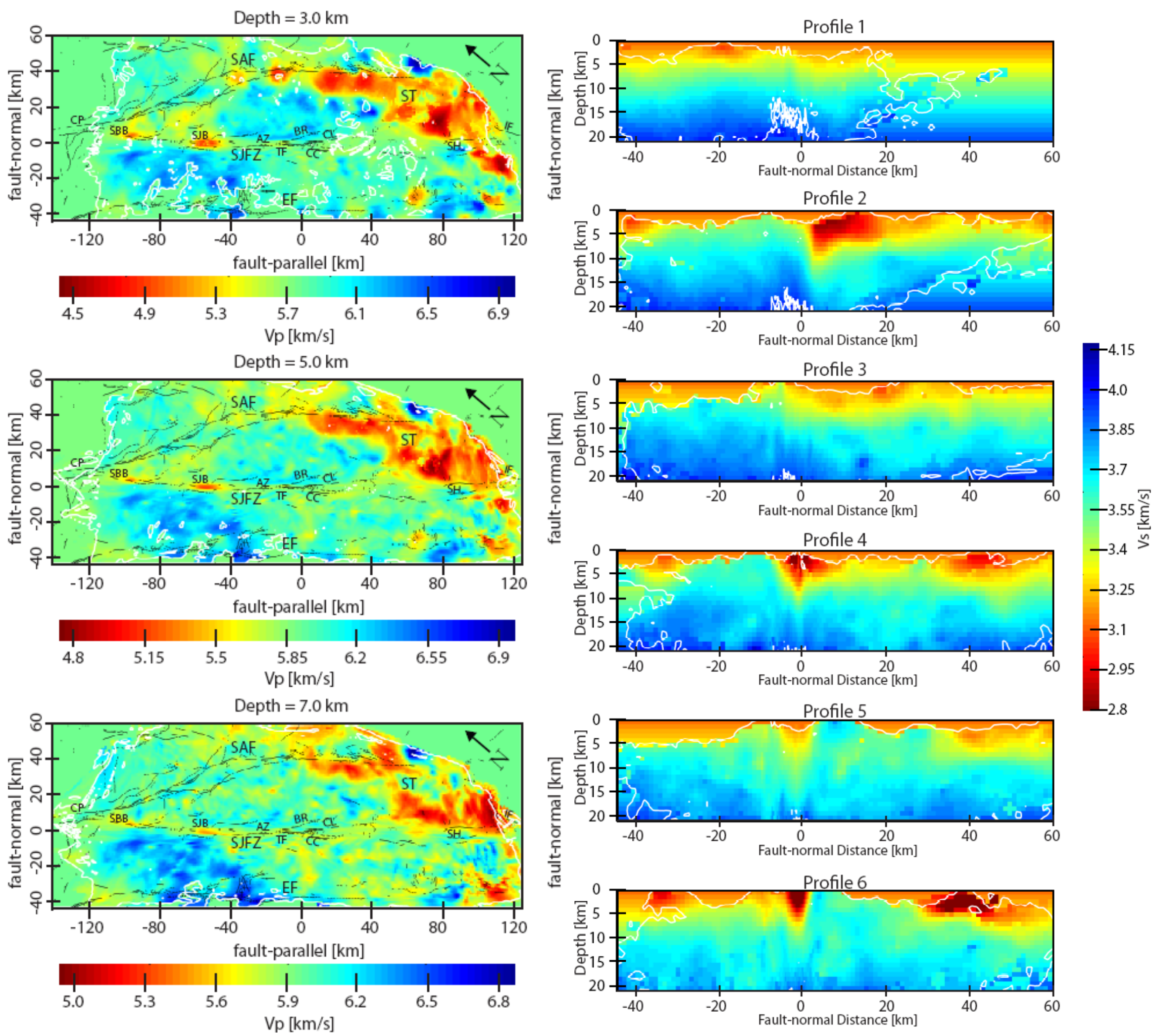

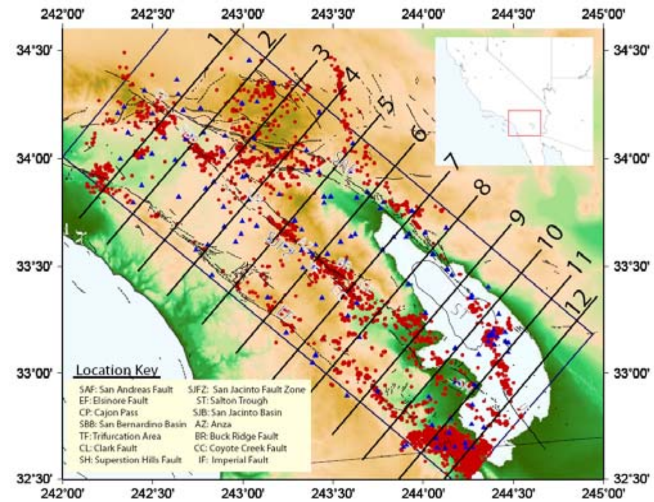

-5493 earthquakes (2000-2011)
-139 stations
-360,000 *P*- and *S* arrival times
-grid cell size: 1km
-white contours > 10 rays/cell

-Follow overall "flower" shape with depth
-Hallows of mild damage extend to 10-15 km
-Larger reductions of Vs (up to 40% in top 3-5 km) than Vp

Clear velocity contrasts (bimaterial interfaces?) in different sections; polarity flips NW of SJB.

Complementary noise-based results for the top 0.5-7 km are given by Zigone et al. (PAGEOPH, 2015).

Internal components of the SJFZ are imaged with fault zone head and trapped waves (next slides).

Properties of the top 0.5 km are imaged and monitored with high-frequency data (later slides).

Fault zone head and trapped waves

Ben-Zion, 1989, 1990

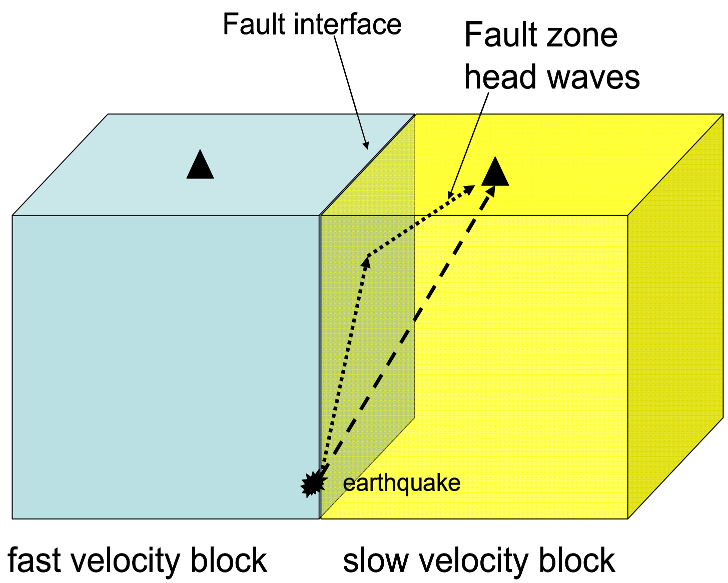

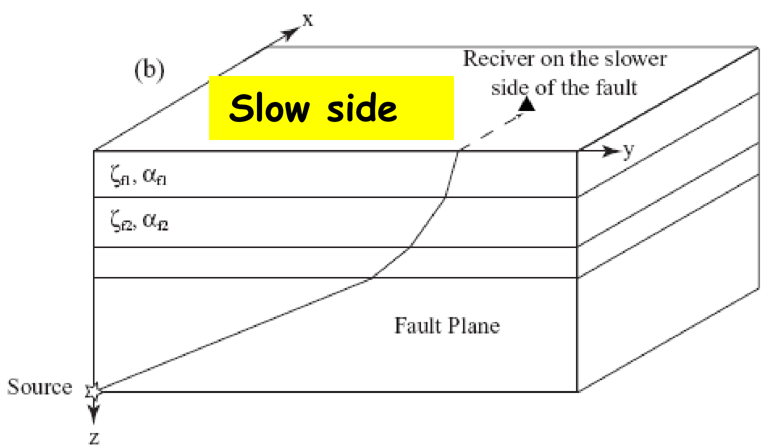

The head waves are first arrivals on slow side positions $x < x_c = r \tan[\cos^{-1}(\alpha_2/\alpha_1)]$

Ben-Zion and Aki, 1990

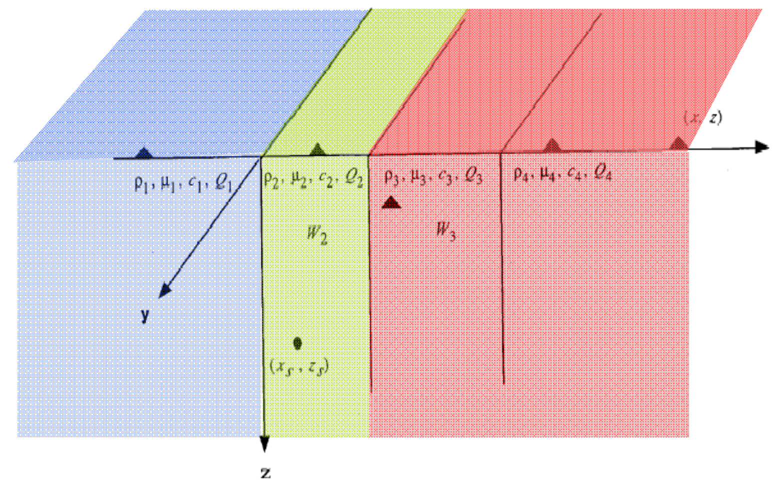

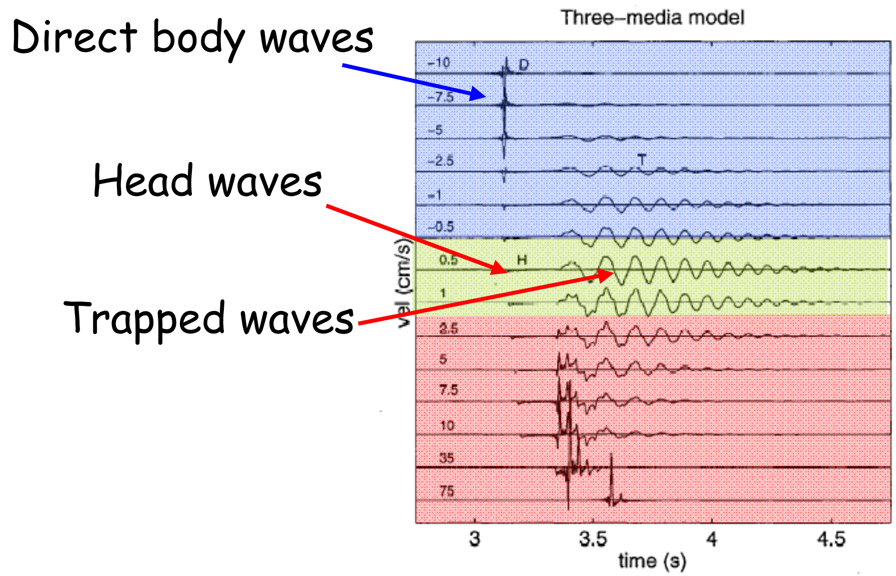

Trapped waves depends strongly on

$$N = r/[W \tan(\theta_c)] = r/[W \tan(\sin^{-1}(\beta_2/\beta_1))]$$

Fault zone head and trapped waves

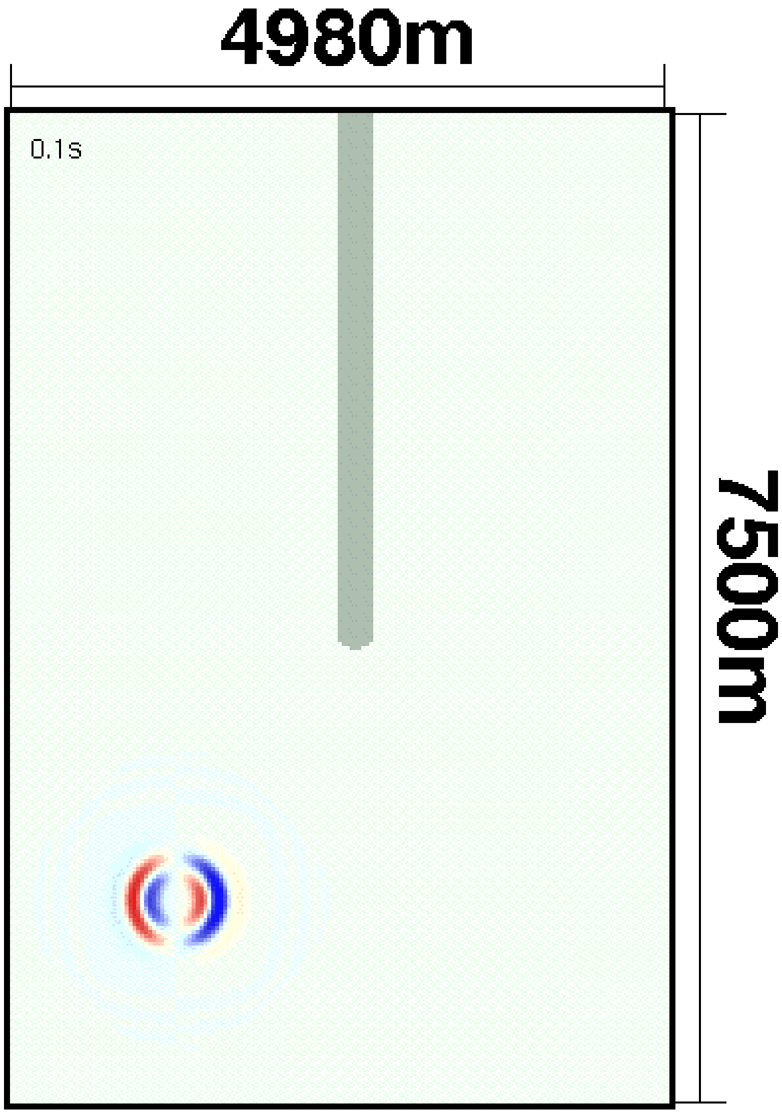

Fohrmann, Igel, Jahnke, Ben-Zion (2004)

Ben-Zion and Aki, 1990

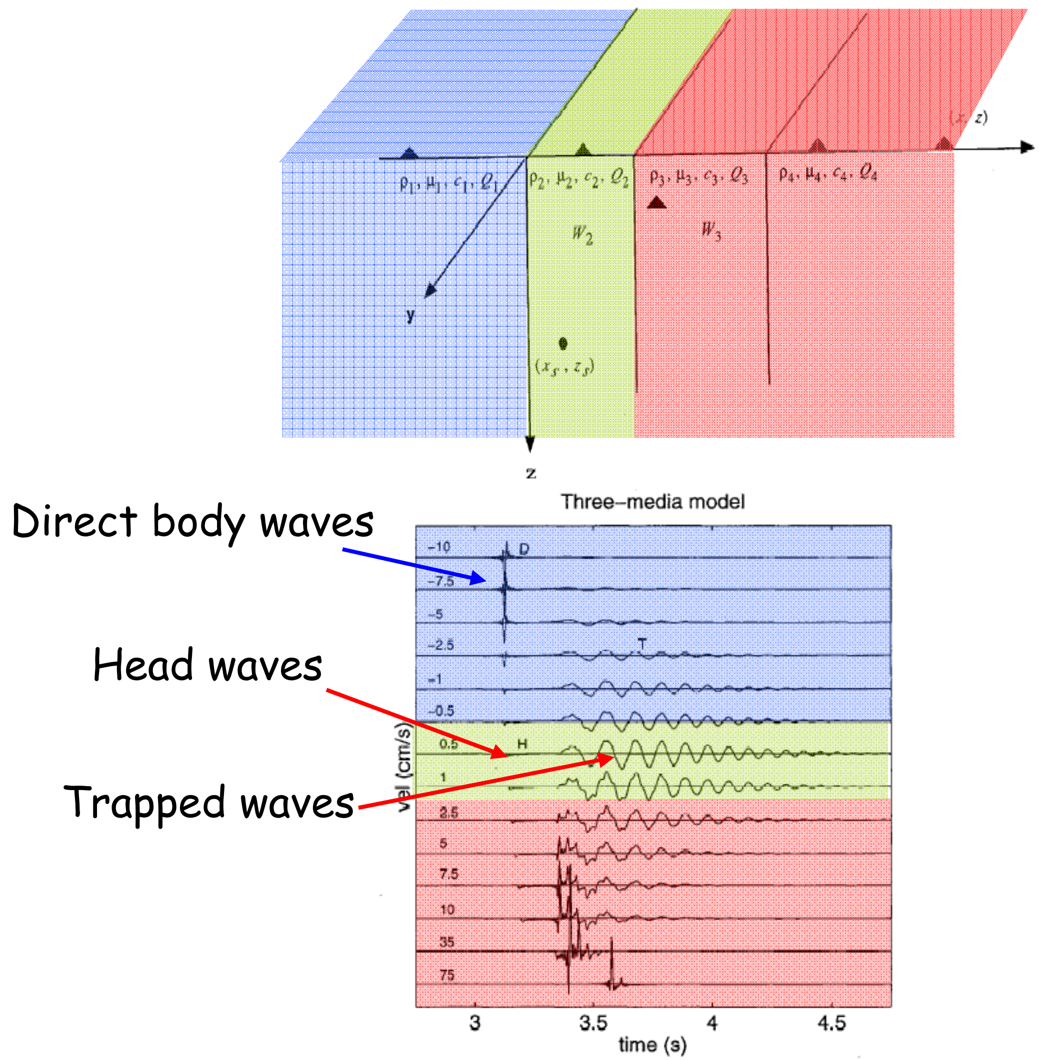

Trapped waves depends strongly on

$$N = r/[W \tan(\theta_c)] = r/[W \tan(\sin^{-1}(\beta_2/\beta_1))]$$

Sage Brush Flats - Clark Fault

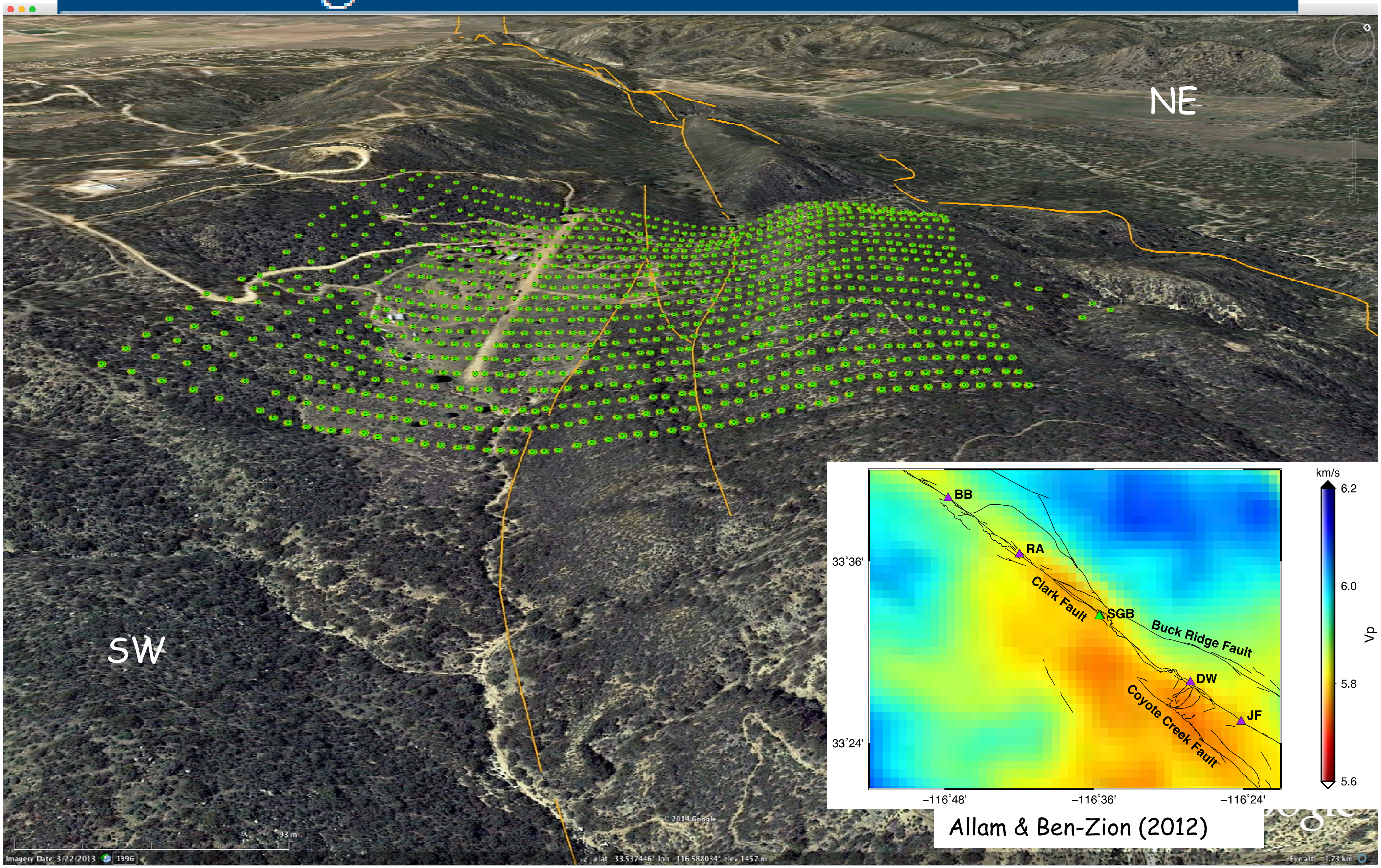

Waveform changes at column 32: Seismogenic Clark fault

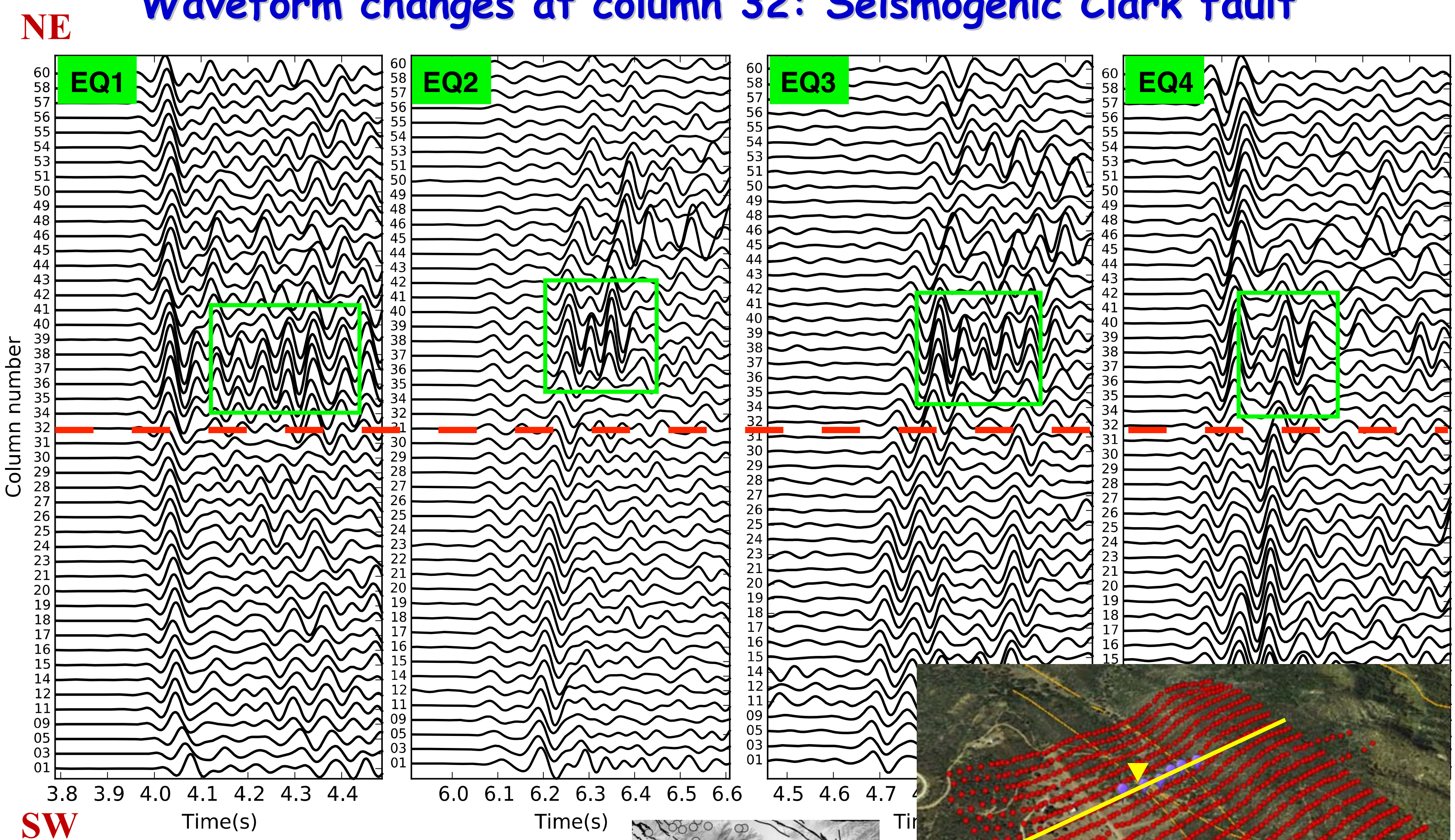

Core damage zone: Column 36-40

Local reversal of velocity contrast!

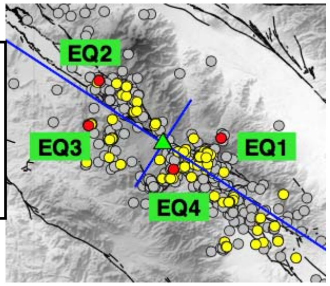

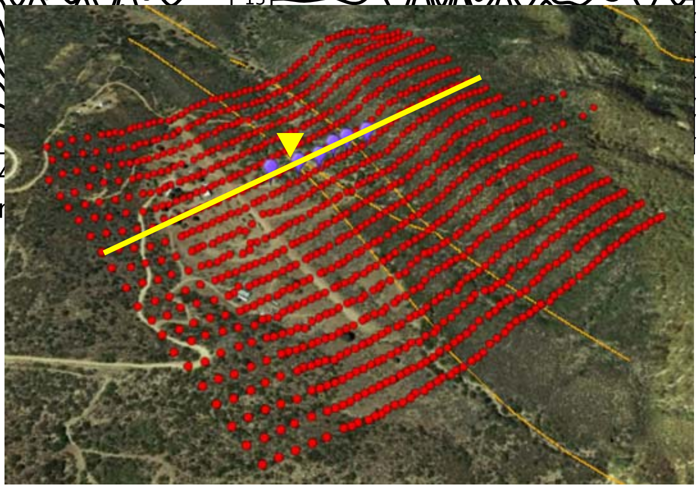

Delay times of P waves and trapped waves indicate a local reversal of the velocity structure

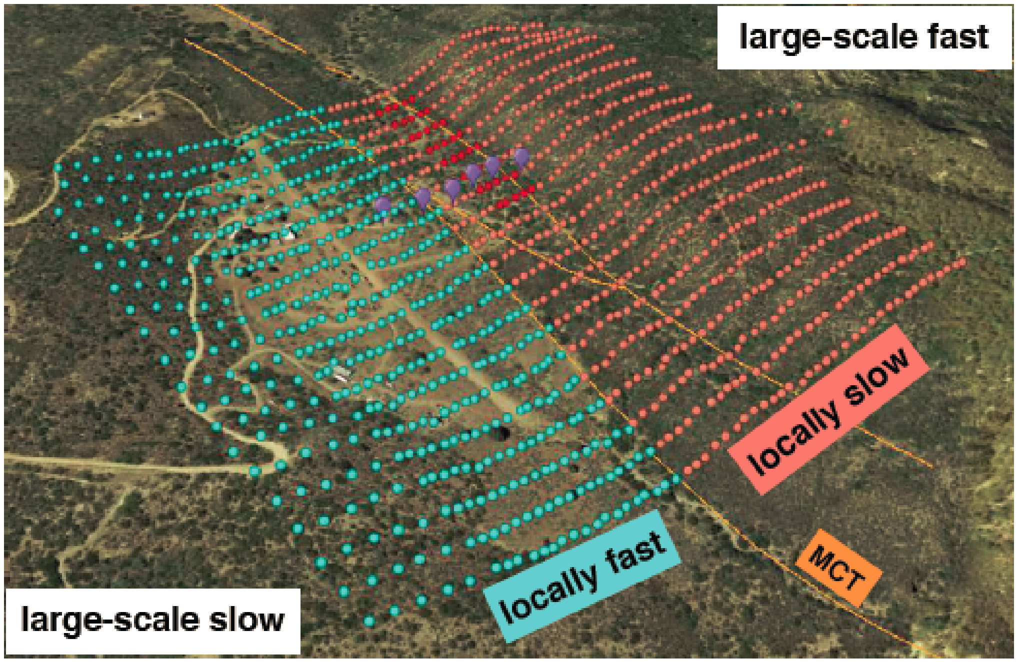

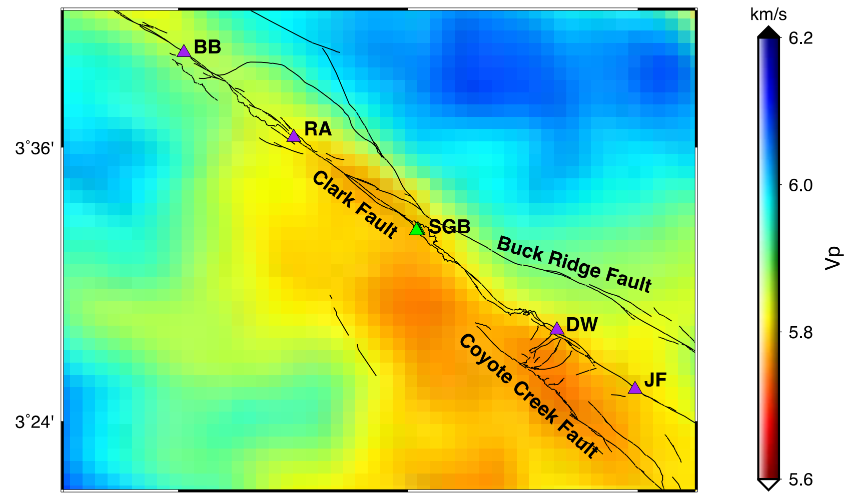

Allam & Ben-Zion (2012)

The large scale velocity contrast and local reversal (damage asymmetry) across the fault indicate preferred direction of earthquake ruptures to the NW (toward Riverside, away from San Diego)

Detailed imaging of the internal fault zone structure (Hillers et al., 2016; Roux et al., 2016, 2017).

Expected damage patterns generated by earthquakes

Dynamic rupture on a frictional fault with off-fault plastic yielding

Homogenous solid: bilateral crack ruptures

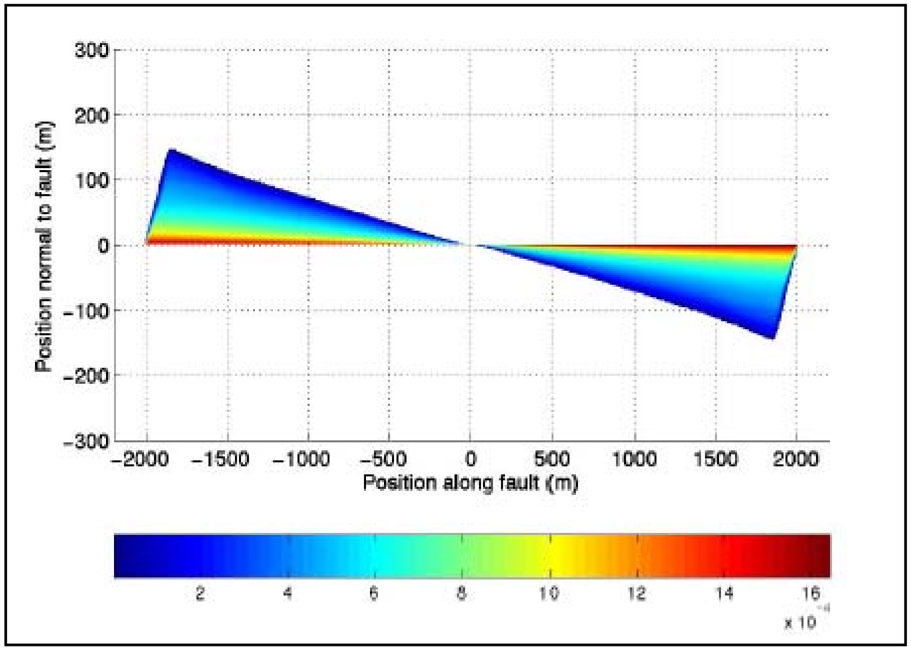

Andrews, 2005

Bimaterial interface: unilateral pulse ruptures

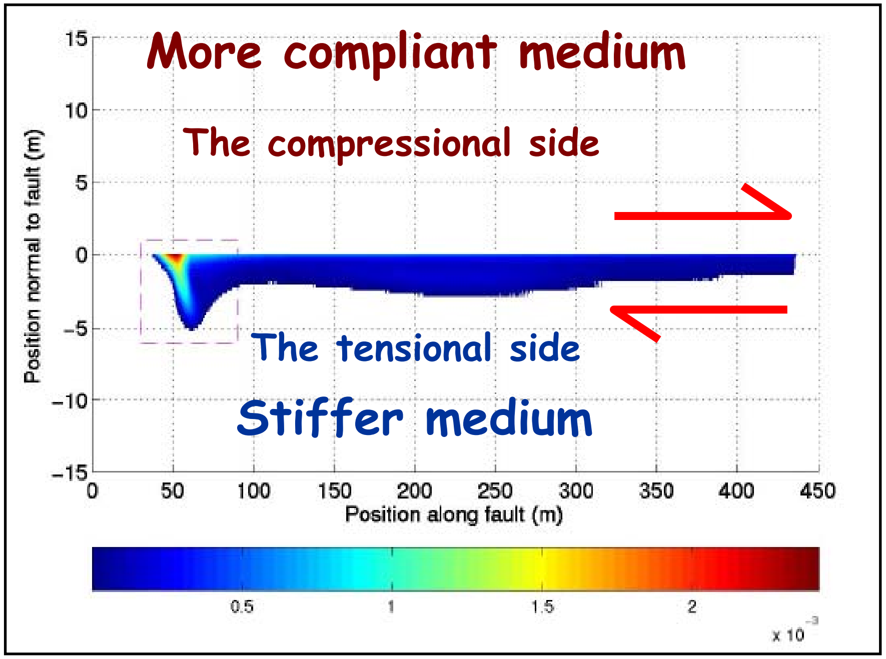

Ben-Zion and Shi, 2005

Analyses of seismic and geological data in several large structures show strongly asymmetric damage zones, producing local reversal of the large-scale contrast, as expected for bimaterial ruptures with persistent directivity (Lewis et al. 2005, 07; Dor et al. 06, 08; Wechsler et al. 09; Mitchell et al. 2011; Rempe et al. 2013; Qiu et al. 2017; Share et al., 2017, ….)

Using focal spot properties for detailed imaging of the subsurface material (Hillers, Roux, Campillo, Ben-Zion, JGR, 2016)

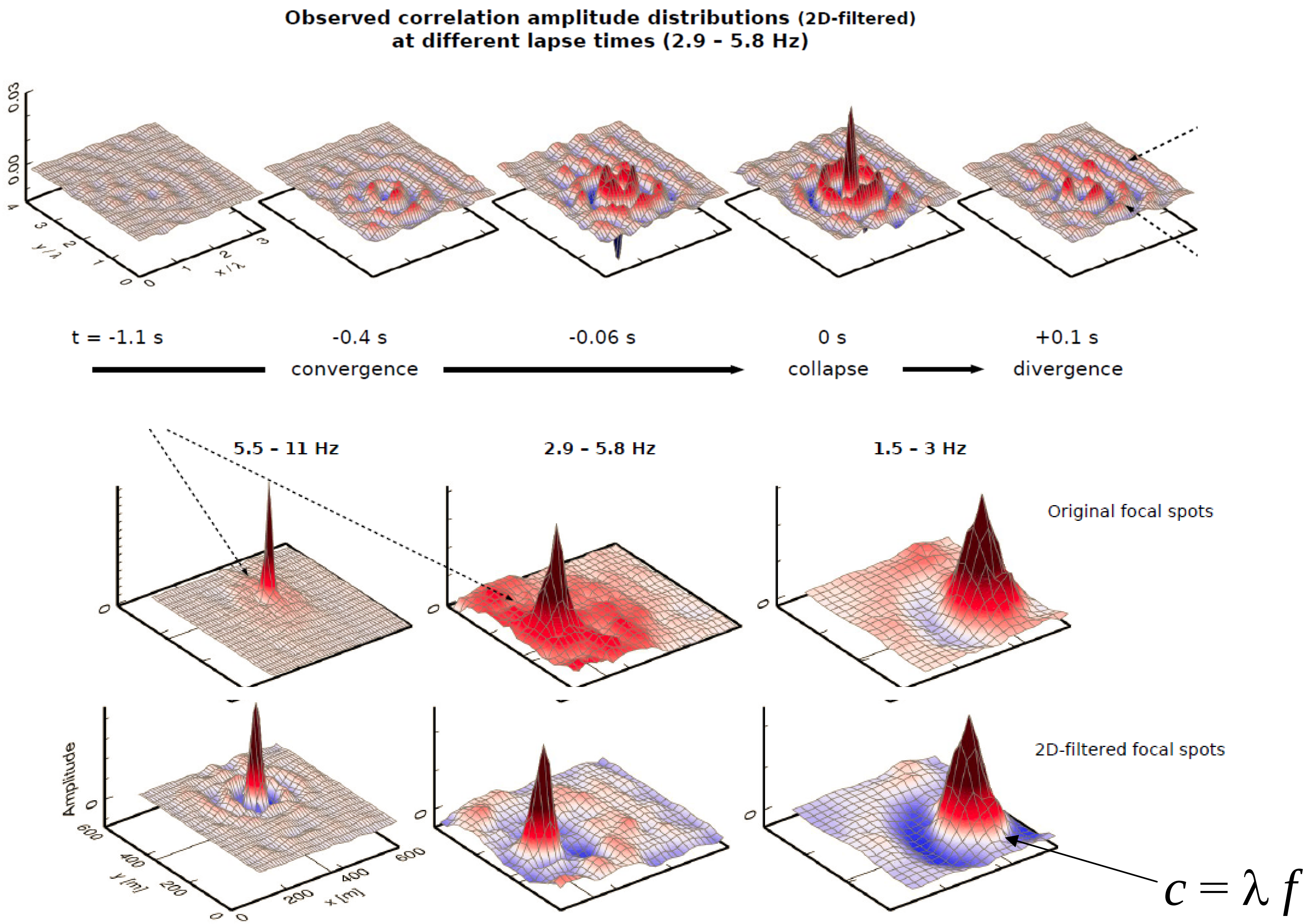

Hillers et al.
JGR, 2016
(c/f ~ 50-500 m)

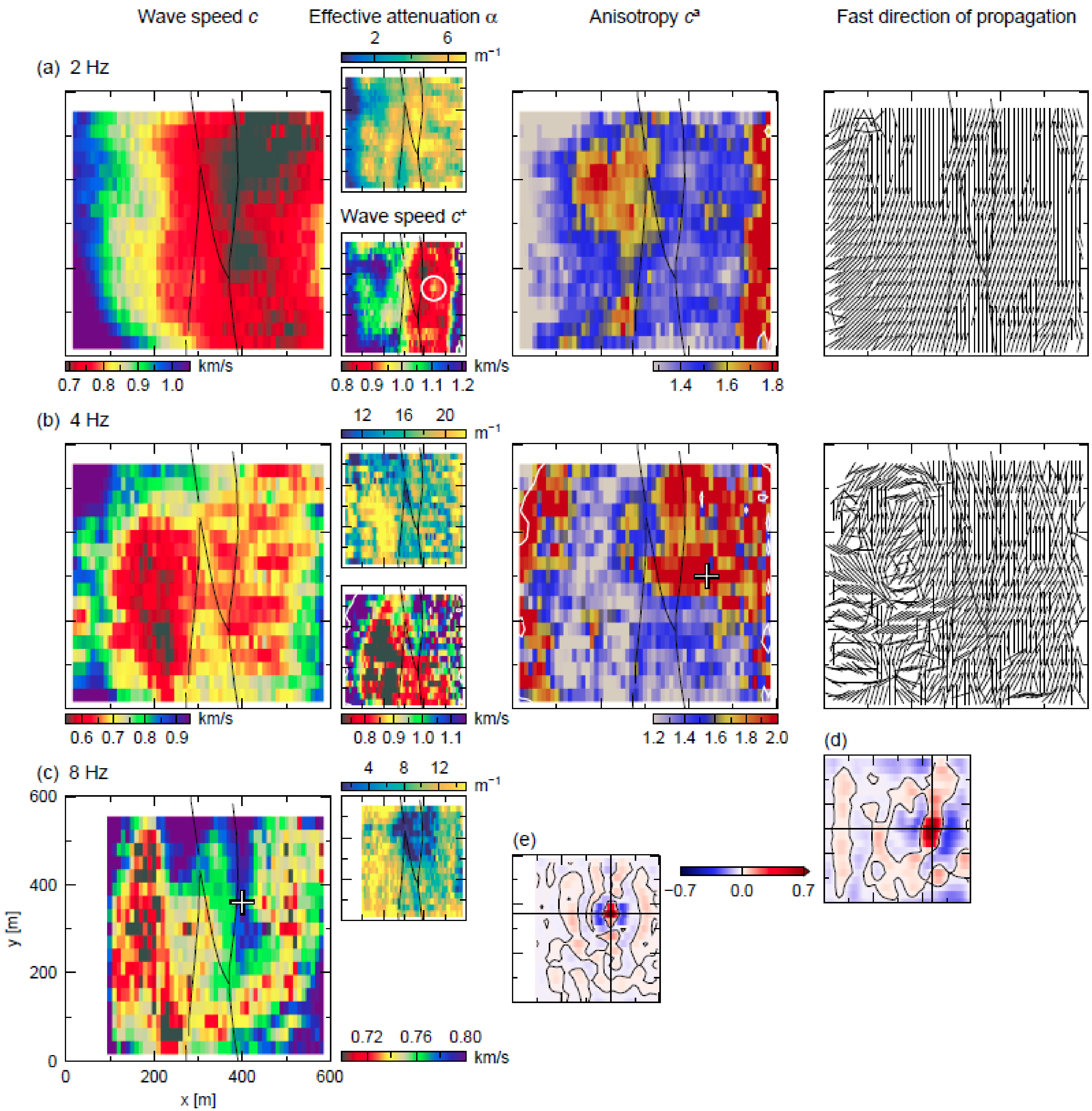

Internal structure of the San Jacinto fault zone at Jackass Flat (JF) from data recorded by a dense linear array (Qiu, et al., GJI, 2017)

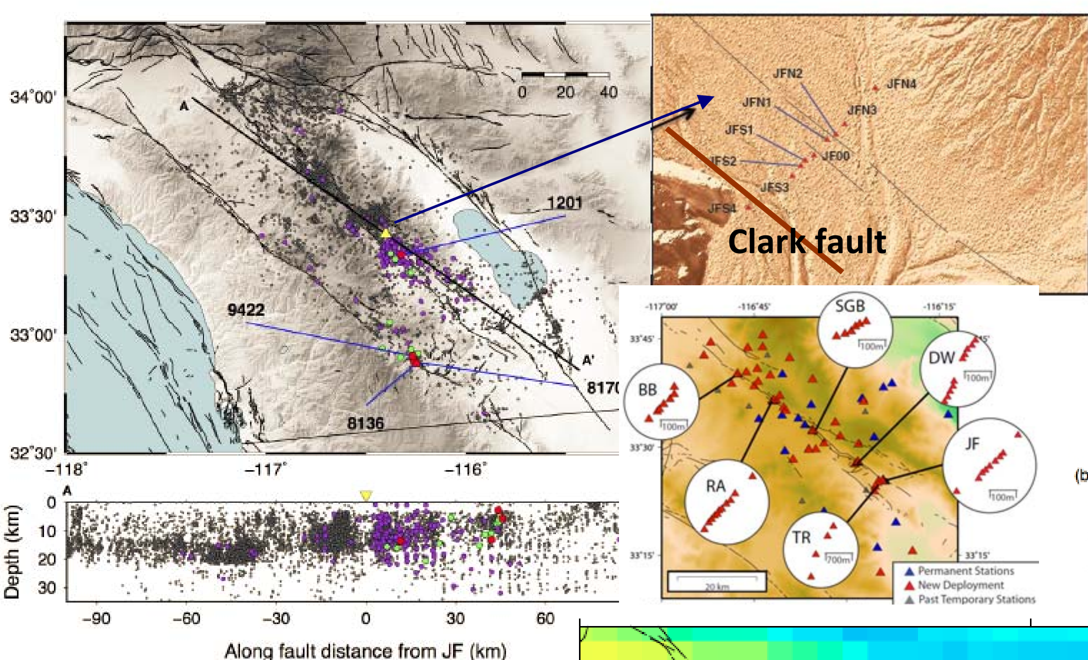

Events generating trapped JF array (colored circles)

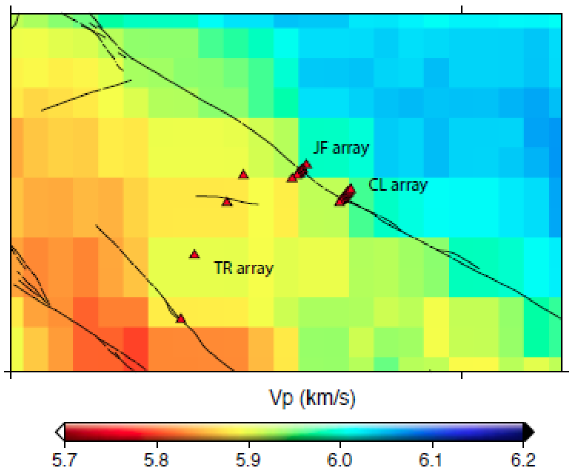

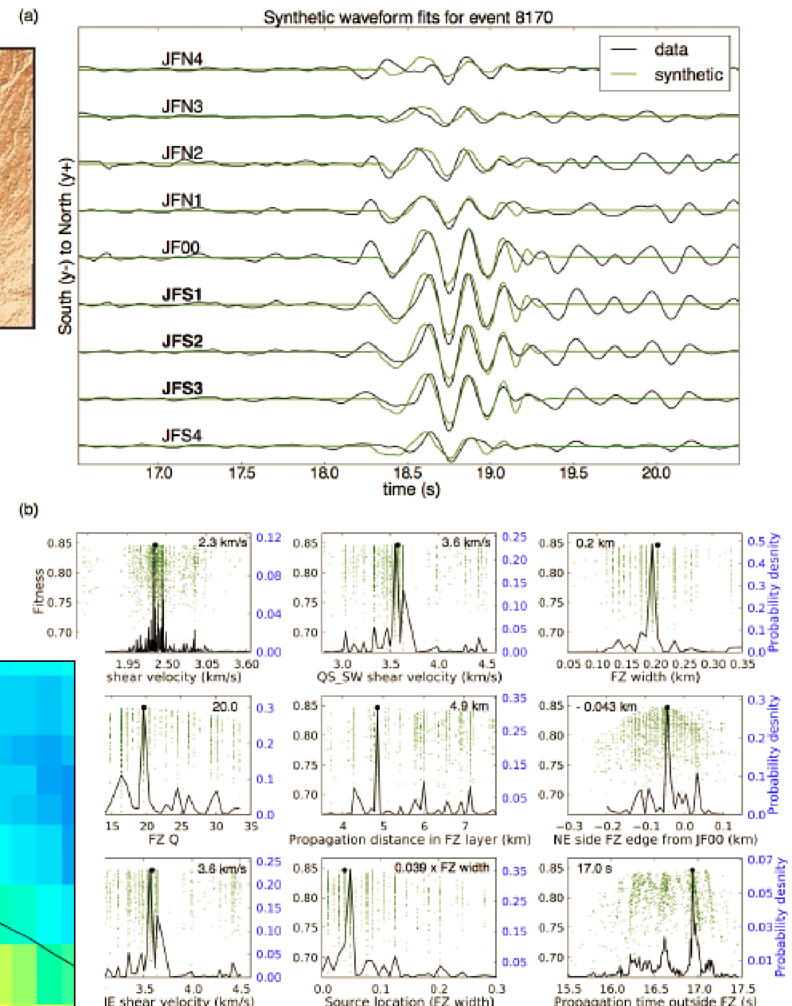

Most likely LVZ parameters:
width ~200 m,
depth ~3.5 km,
S velocity reduction ~50%,
Q-value ~20.

The damage zone is primarily on the side with faster Vs at depth; consistent with preferred earthquake ruptures to the NW

Top: synthetic waveform fits.

Bottom: parameter-space results of genetic inversion algorithm.

Internal structure of the San Jacinto fault zone at Blackburn Saddle from a dense linear deployment across the fault (Share et al., 2017; Allam et al., 2017)

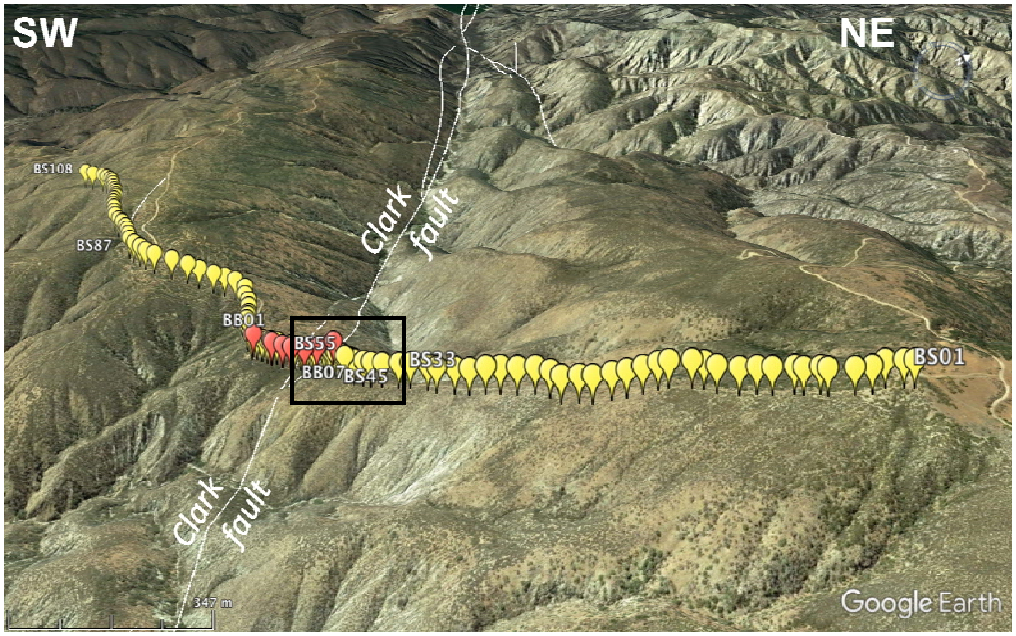

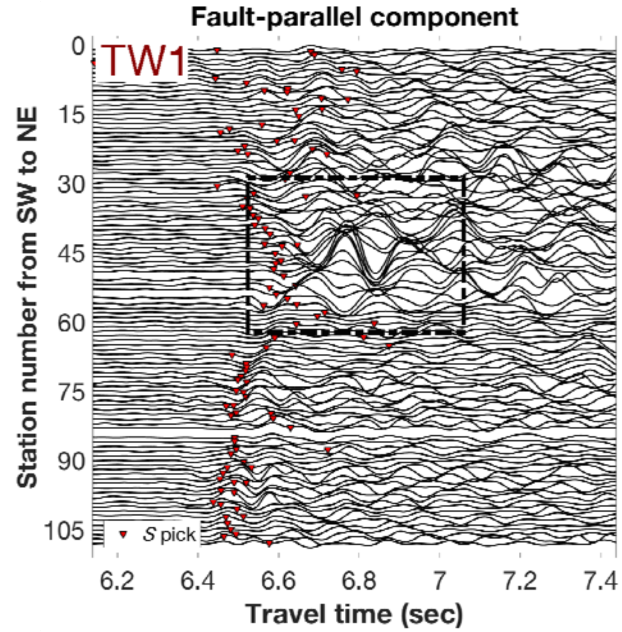

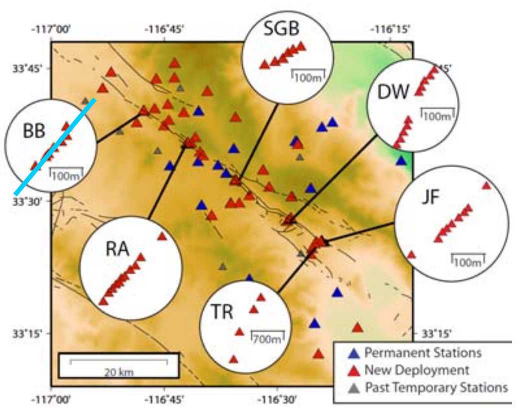

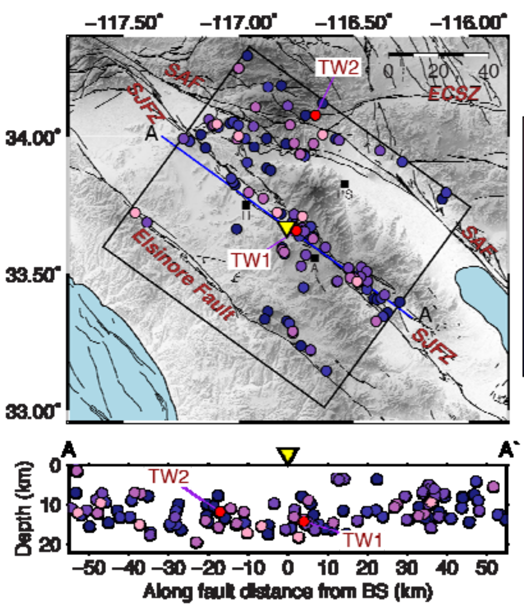

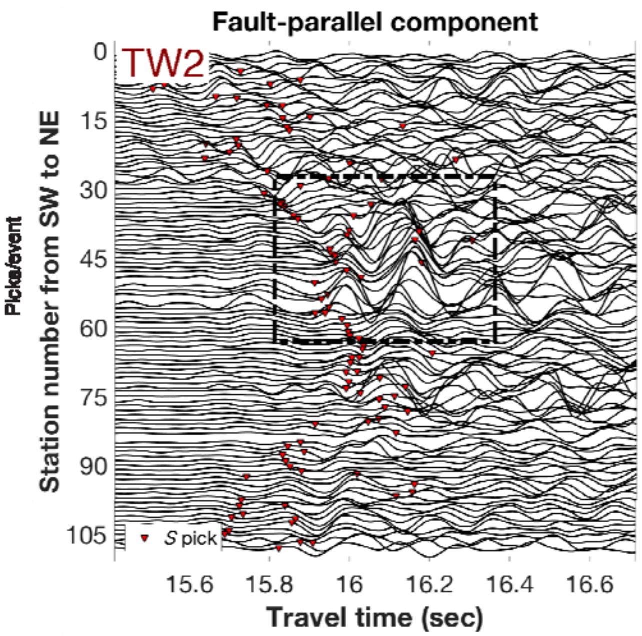

Large-scale structure across the fault

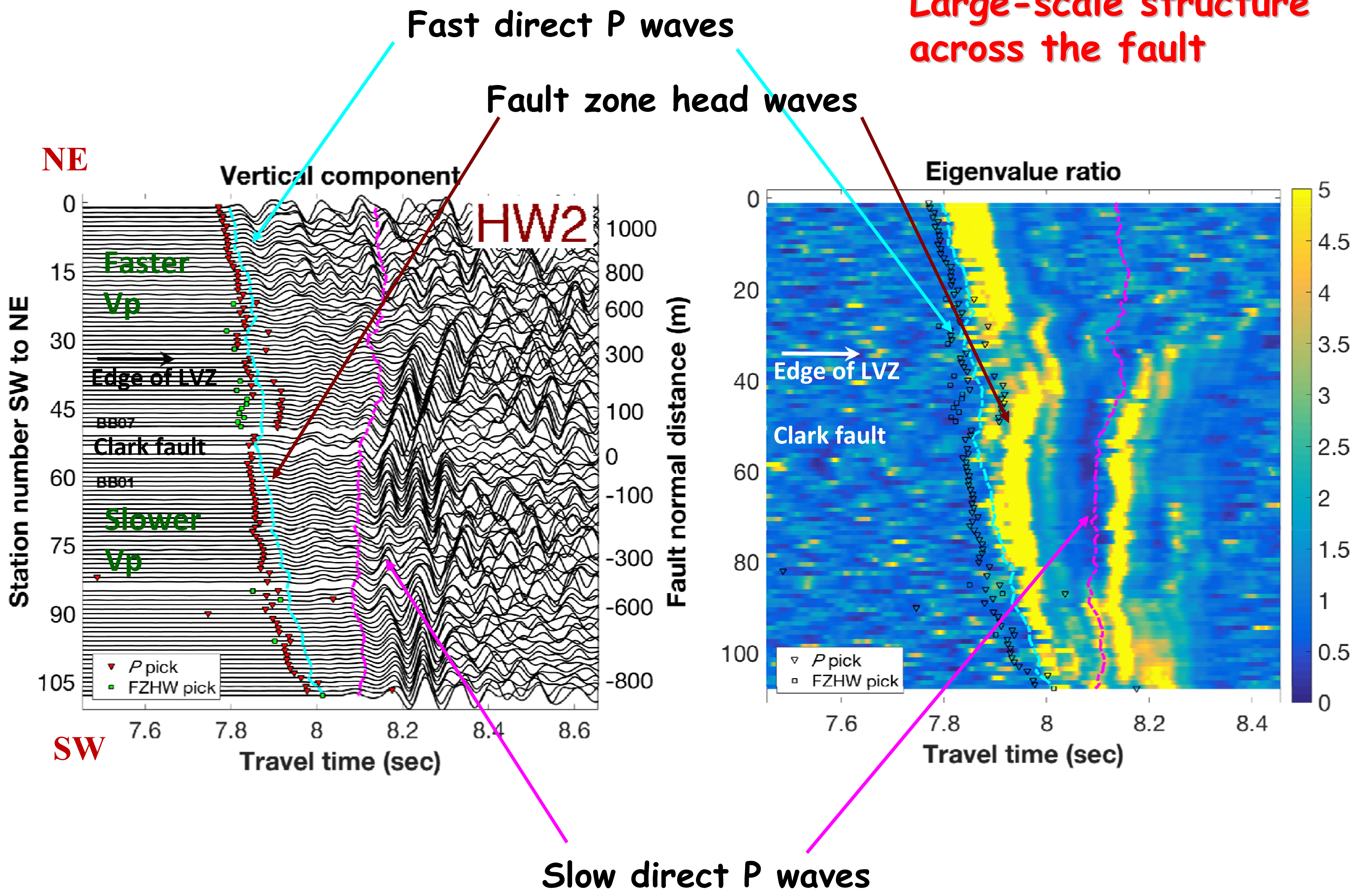

Average 10% velocity contrast across the SJFZ from trifurcation area to the BB array

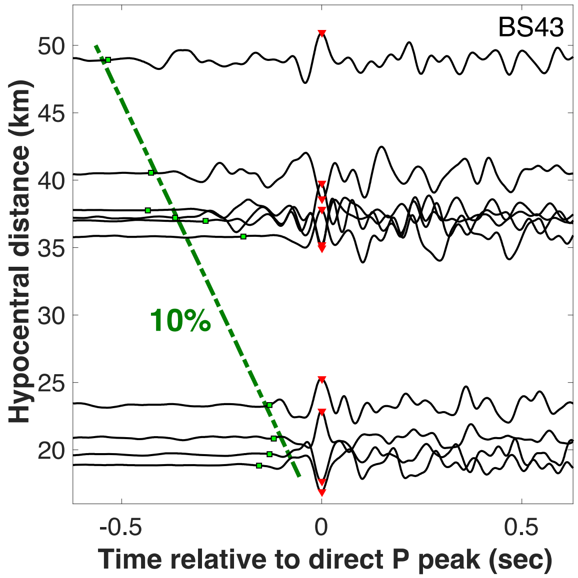

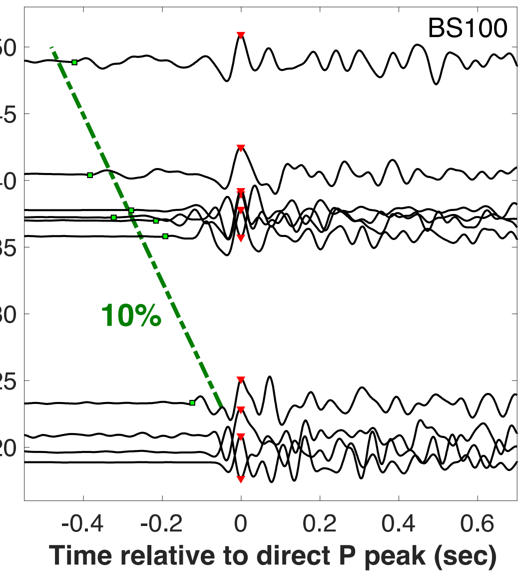

$$\Delta t \approx r \Delta\alpha / \alpha^2$$

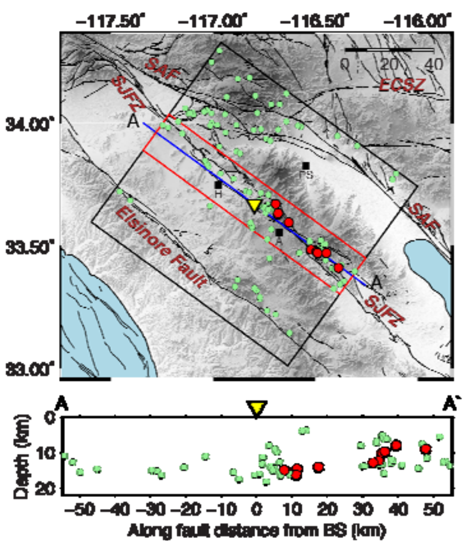

Damage asymmetry (offset to the fast block)

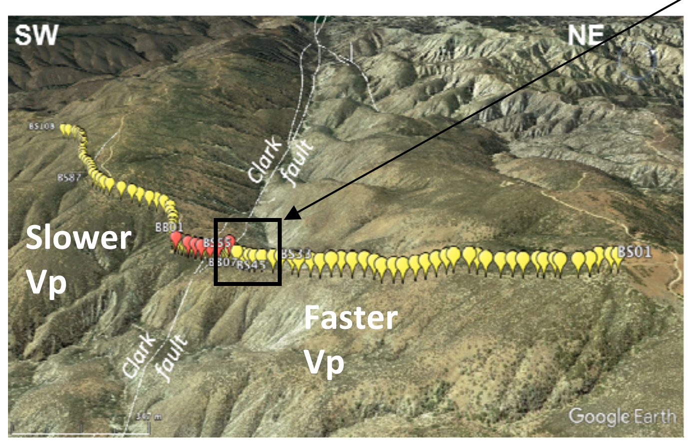

The large scale velocity contrast and local reversal (damage asymmetry) indicate preferred direction of earthquake ruptures to the NW

Fault Zone Resonance (Allam et al., 2017)

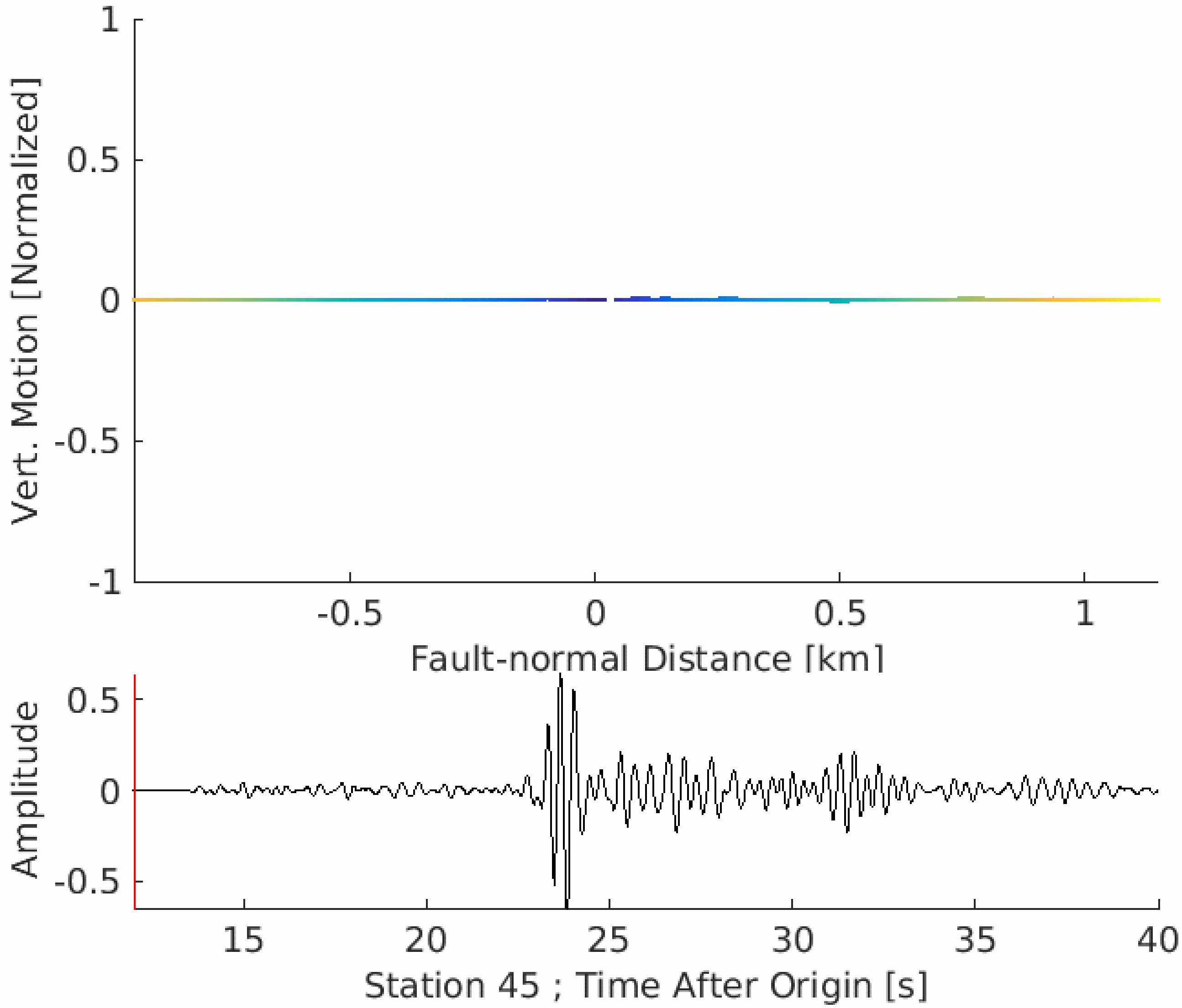

Average maximum amplitude for 278 events

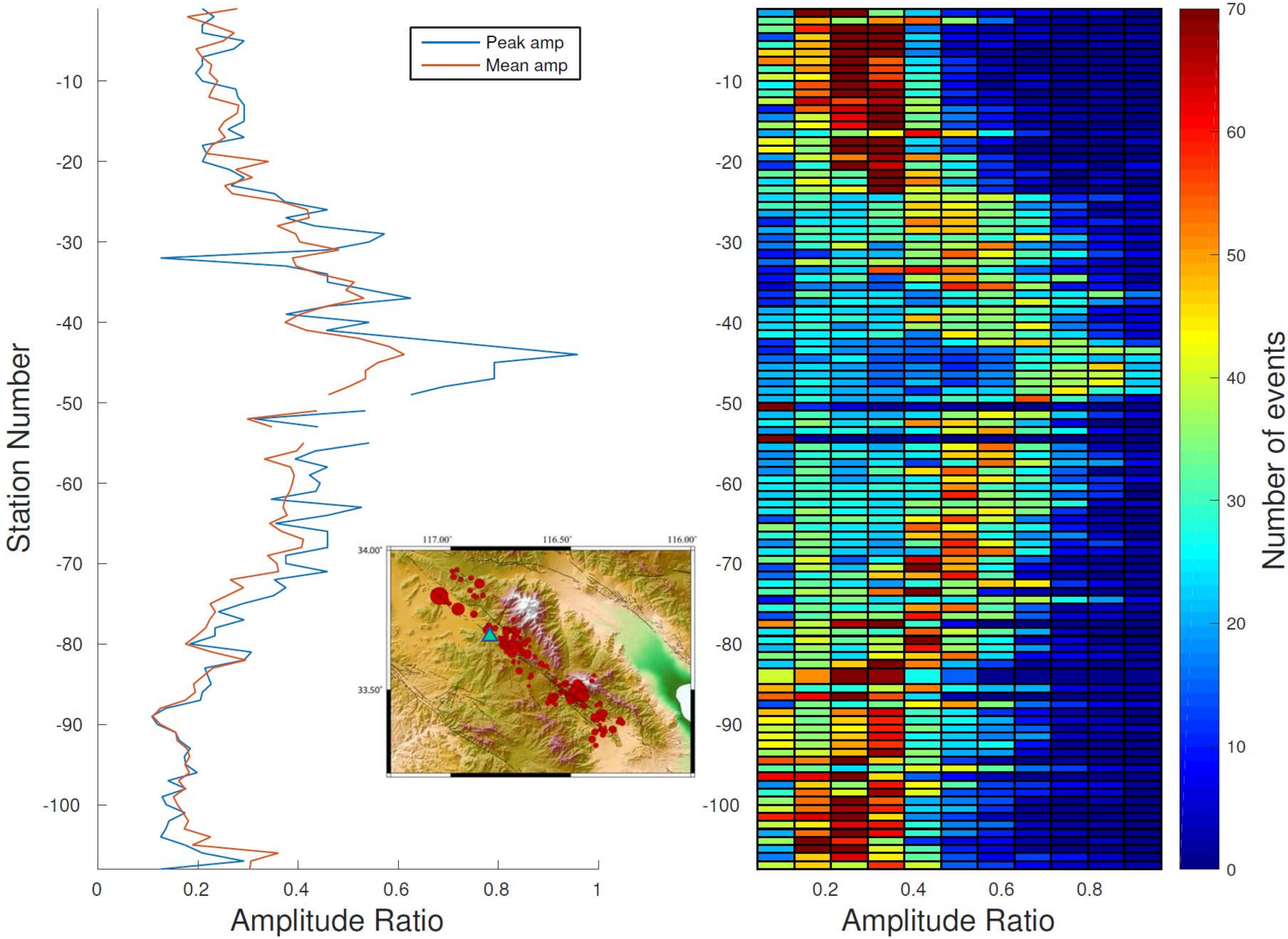

Vertical Low Velocity Zone Normal Modes

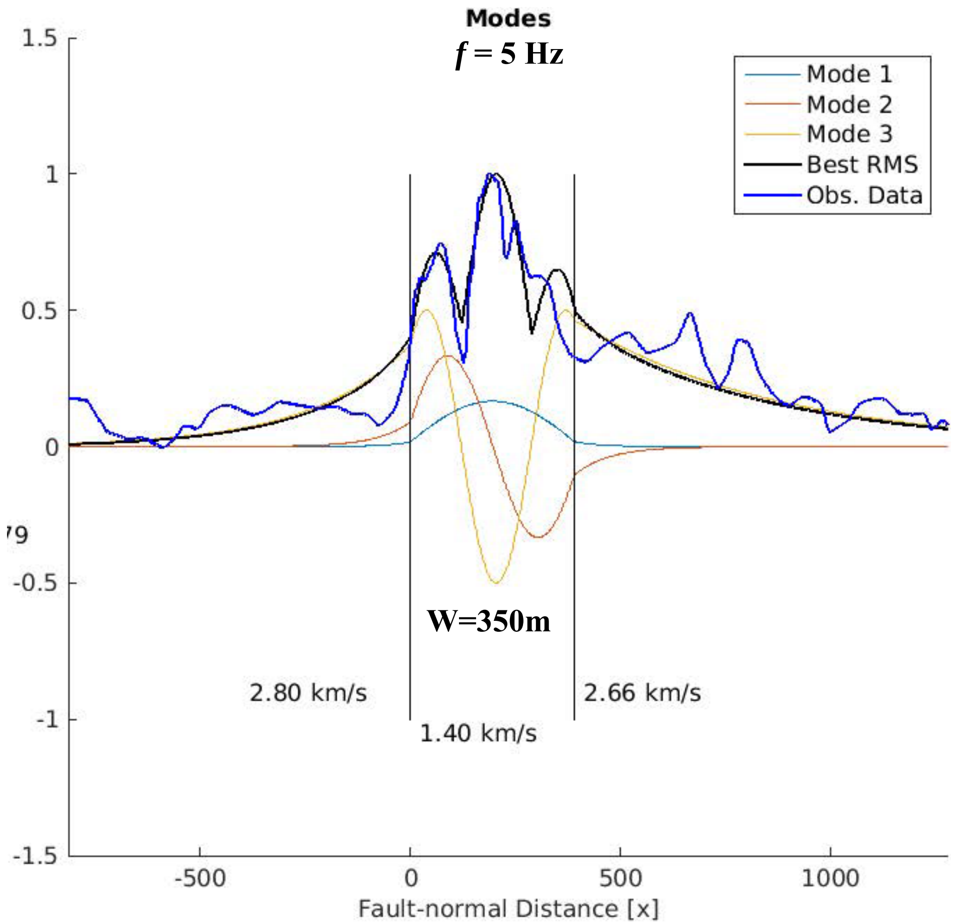

Ben-Zion and Aki, 1990

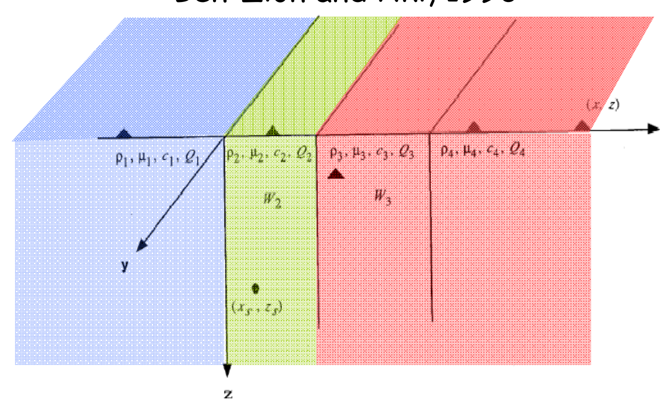

$$\tan[w\omega({\beta_2}^{-2} - c^{-2})^{1/2}]$$
$$= \frac{\mu_2({\beta_2}^{-2} - c^{-2})^{1/2}[\mu_1(c^{-2} - {\beta_1}^{-2})^{1/2} + \mu_3(c^{-2} - {\beta_3}^{-2})^{1/2}]}{{\mu_2}^2({\beta_2}^{-2} - c^{-2}) - \mu_1\mu_3(c^{-2} - {\beta_1}^{-2})^{1/2}(c^{-2} - {\beta_3}^{-2})^{1/2}}. \quad (2.9)$$

Temporal changes of seismic velocities

Brenguier et al. 2008

Co- and post-seismic changes at Parkfield

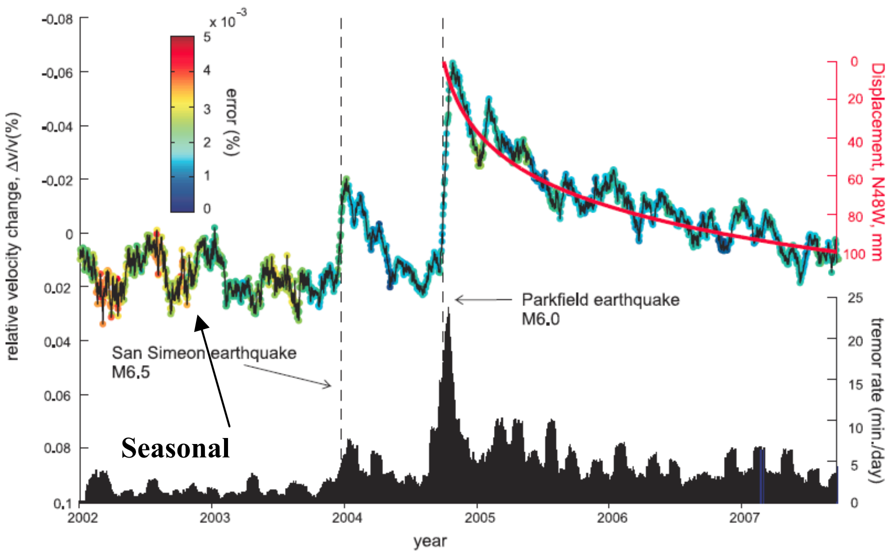

Co-seismic change 0.06%
Time step 30 days

Hillers et al. 2015

Seasonal velocity changes in the SJFZ area

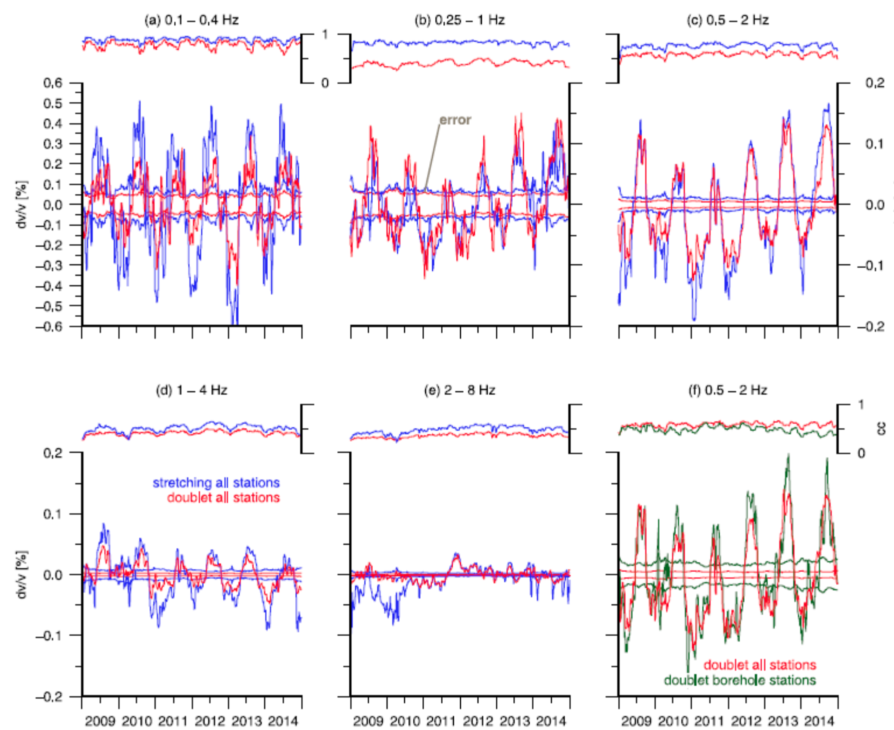

Seasonal changes 0.2%
Time step 10 days

Time steps of seconds reveal co-seismic changes of 30-40% in the shallow crust!

Implications for monitoring deeper changes?

Seismic observations associated with rupture zones along the NAF

(Ben-Zion et al., 03; Peng & Ben-Zion, 04, 05, 06; Wu et al., 09, 10; Lewis & Ben-Zion, 10; Roux & Ben-Zion 14)

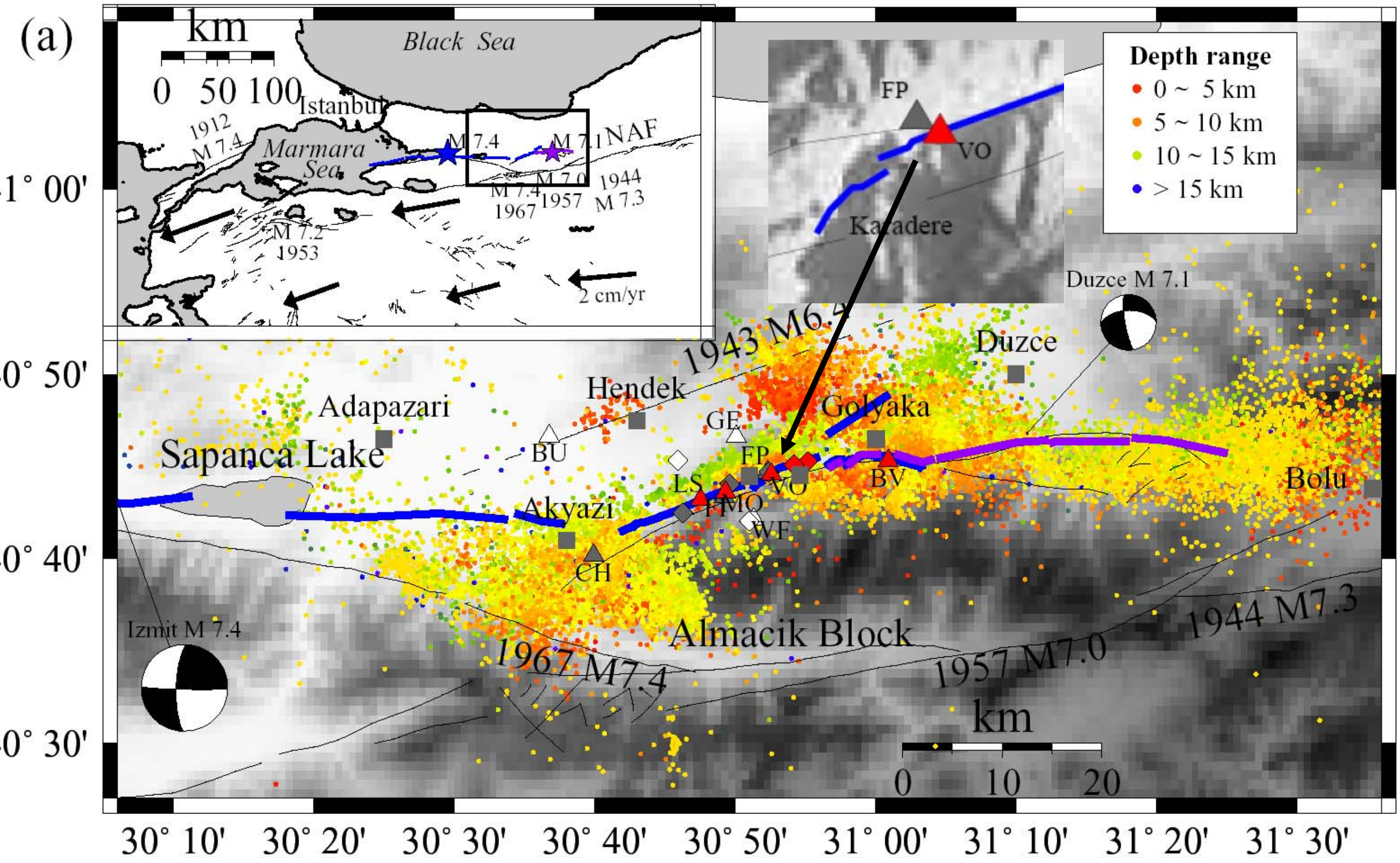

A PASSCAL network along the Karadere-Duzce branch of the NAF recorded ~26000 earthquakes in the 6-months following the 1999 Izmit earthquake

4D analysis of seismic properties along the Karadere-Duzce branch of the NAF (Peng and Ben-Zion, 2004, 2005, 2006)

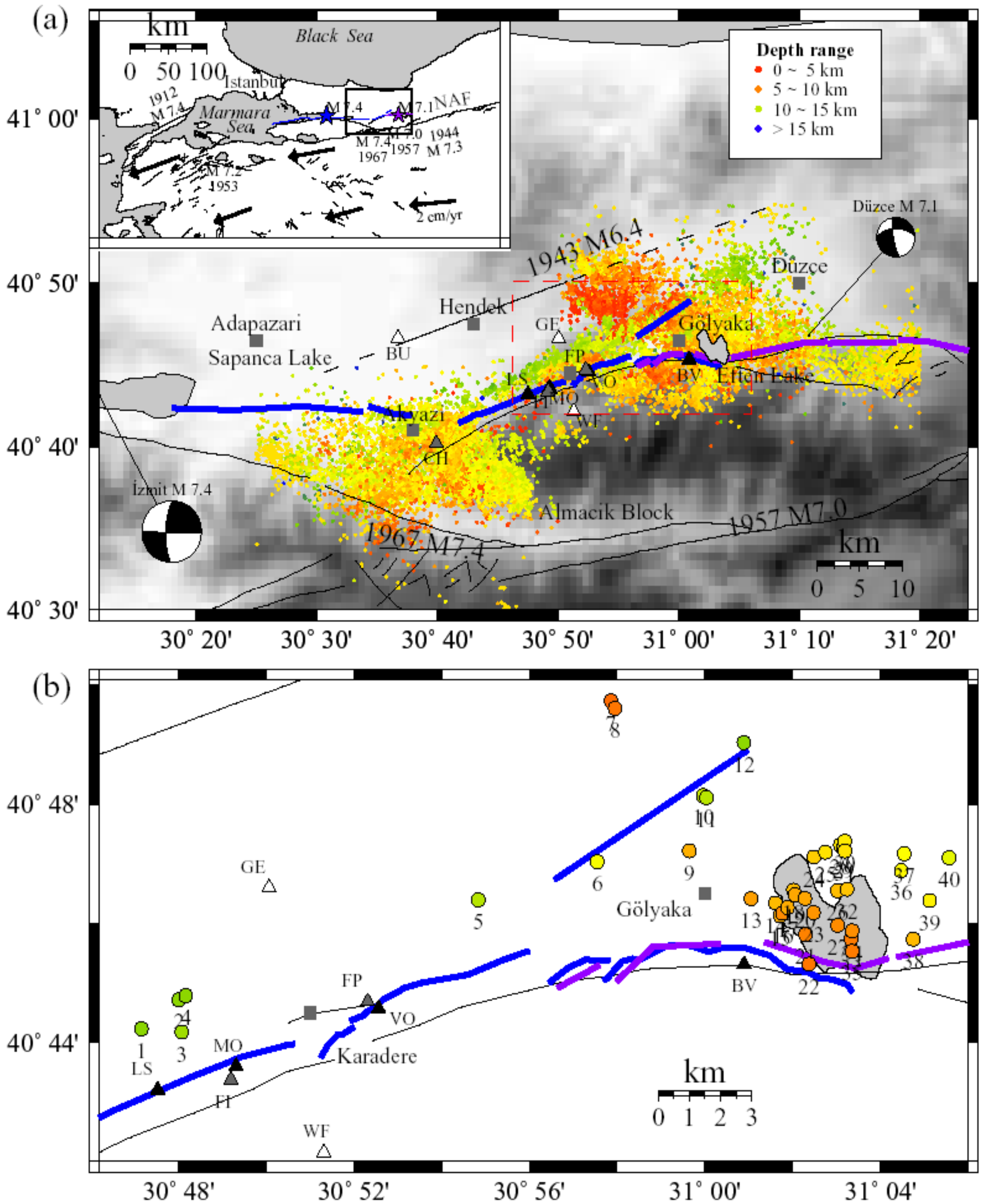

cluster C04, station FP

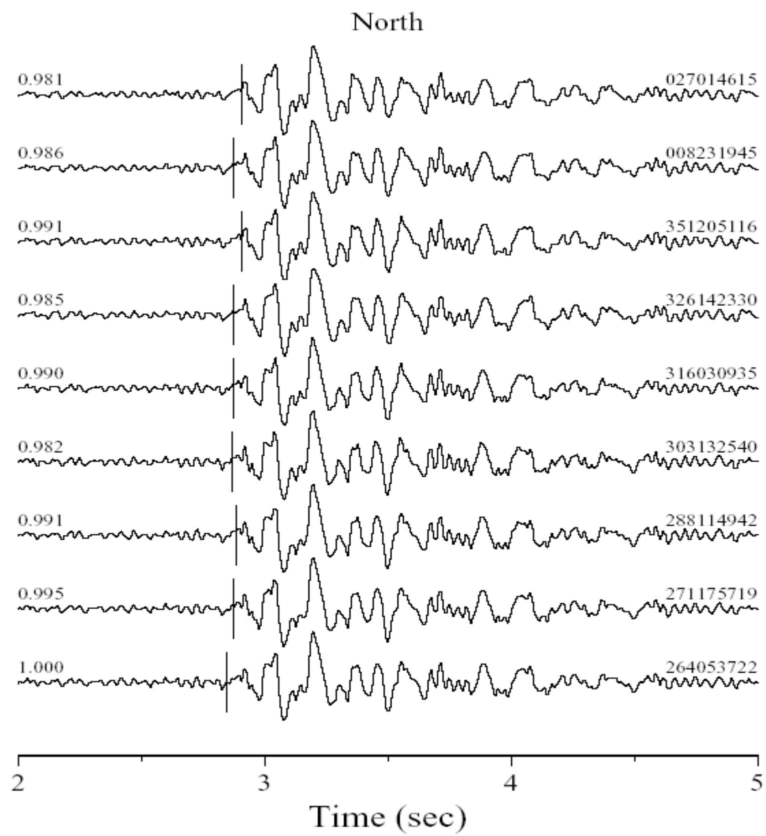

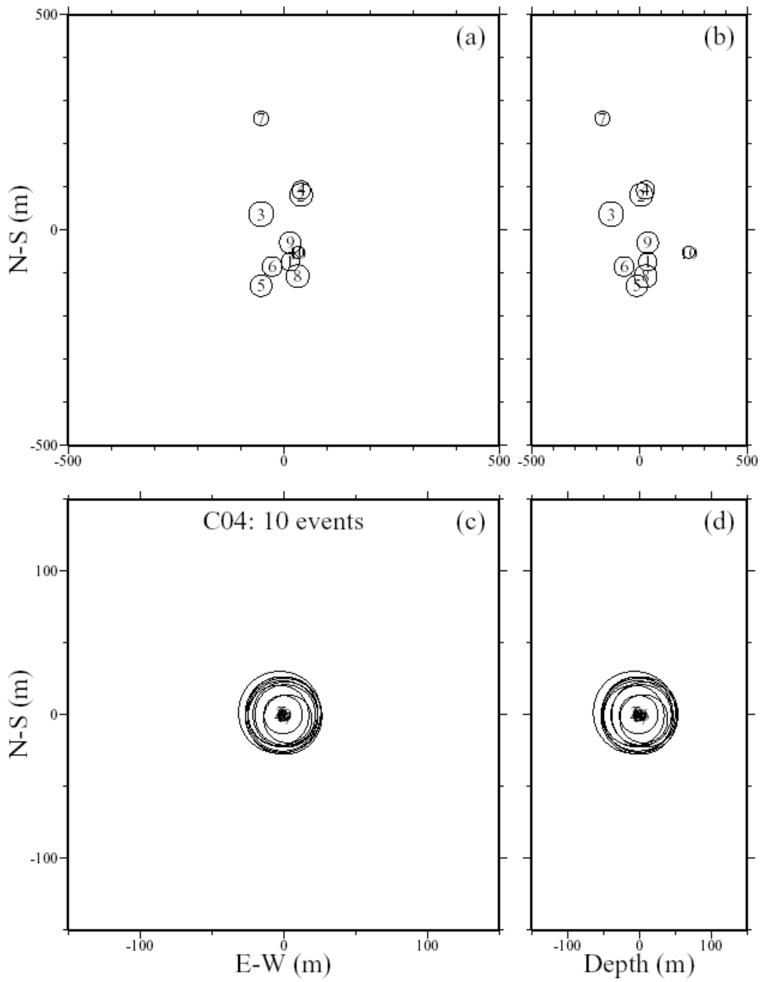

Estimate source areas with

$$r^3 = (7/16)(P_0/\Delta\varepsilon)$$

$$\log P_0 = 1.00M - 4.72$$

with $\Delta\varepsilon = 10^{-4}$

Keep only events with at least 50% overlap of rupture area

Time step of early repeating events minutes to day

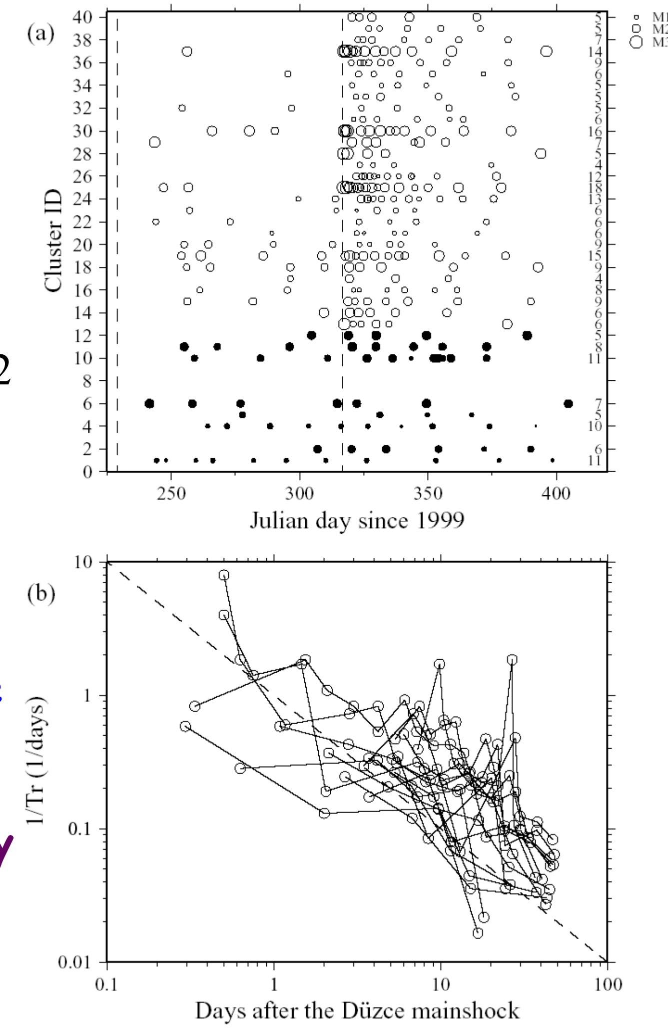

The temporal evolution of events in repeating earthquake clusters follows approximately the Omori law of regional aftershocks

Temporal changes of delay times based on evolving de-correlation analysis

(Peng and Ben-Zion, 2006)

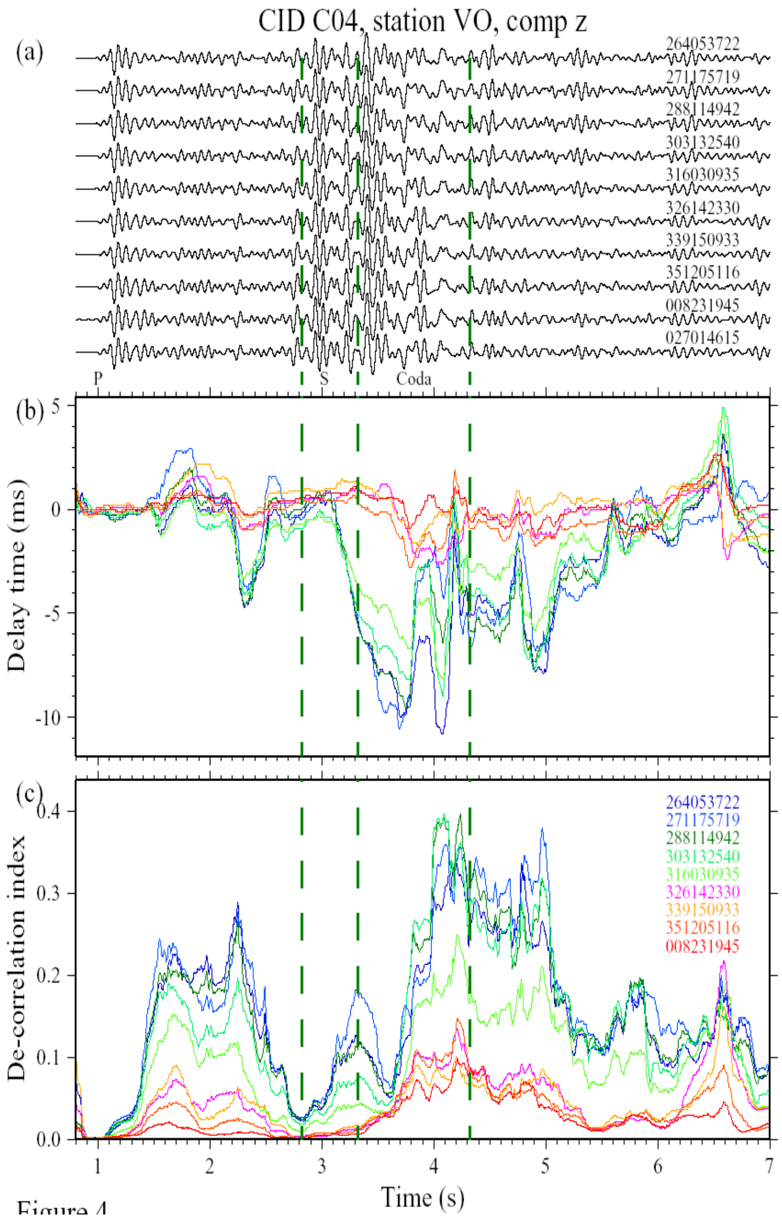

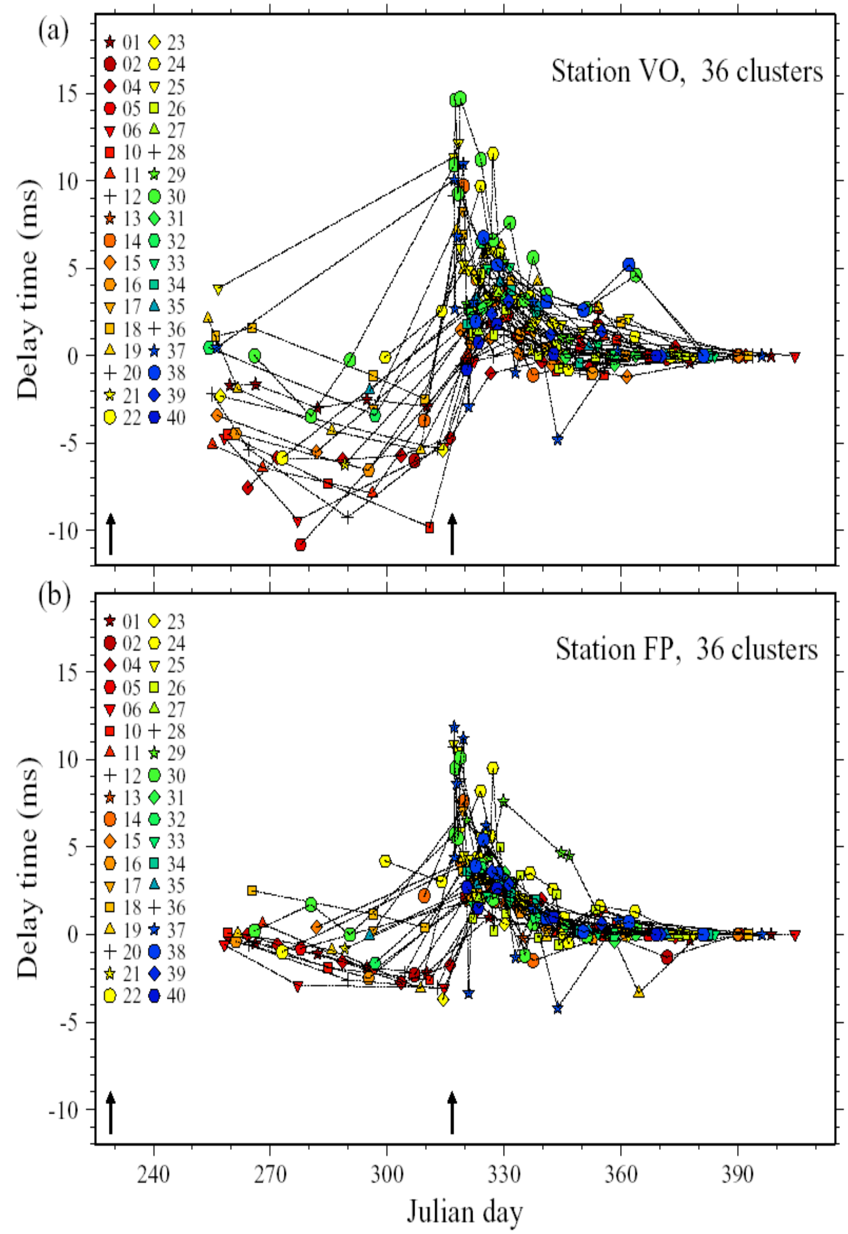

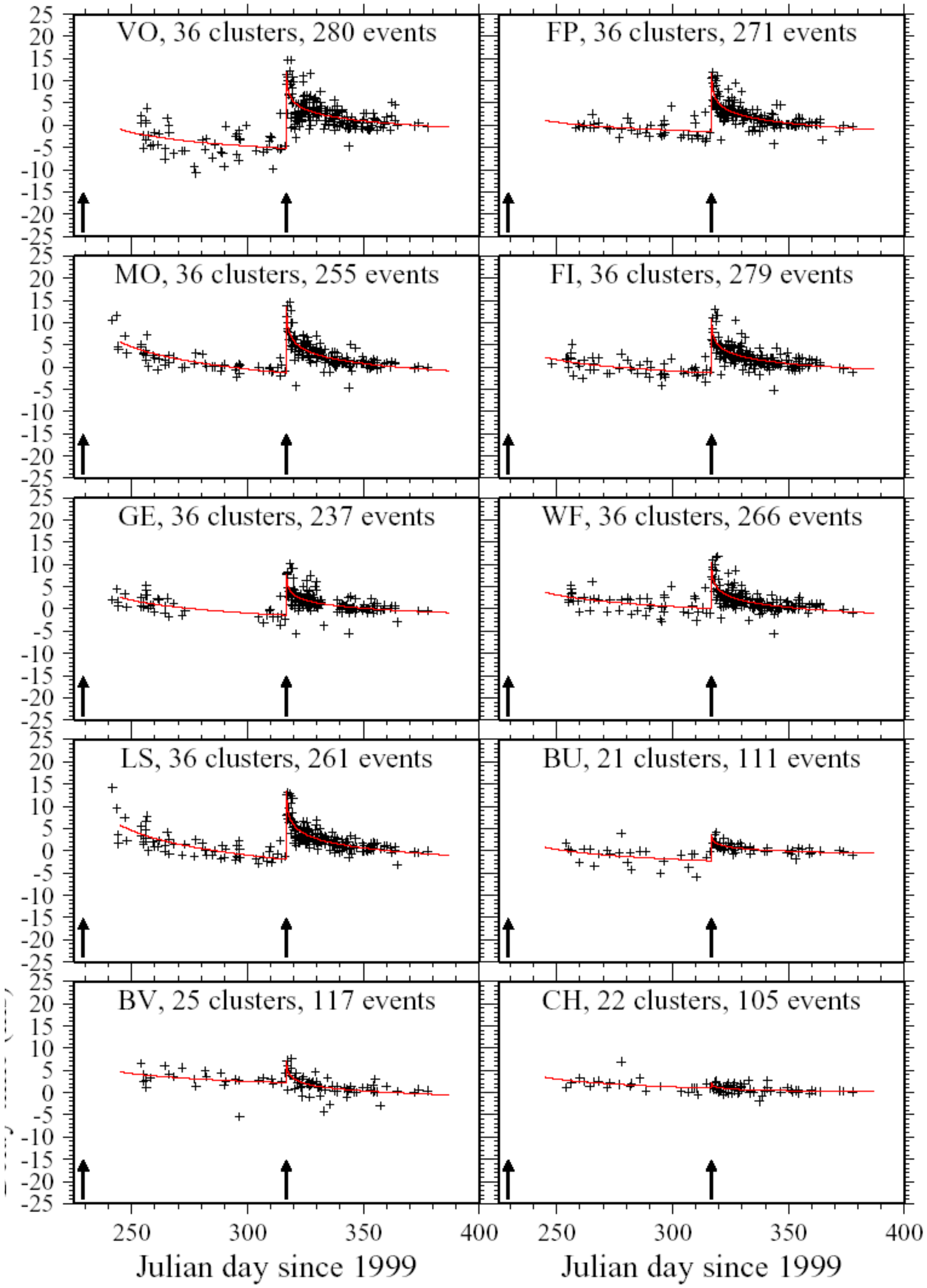

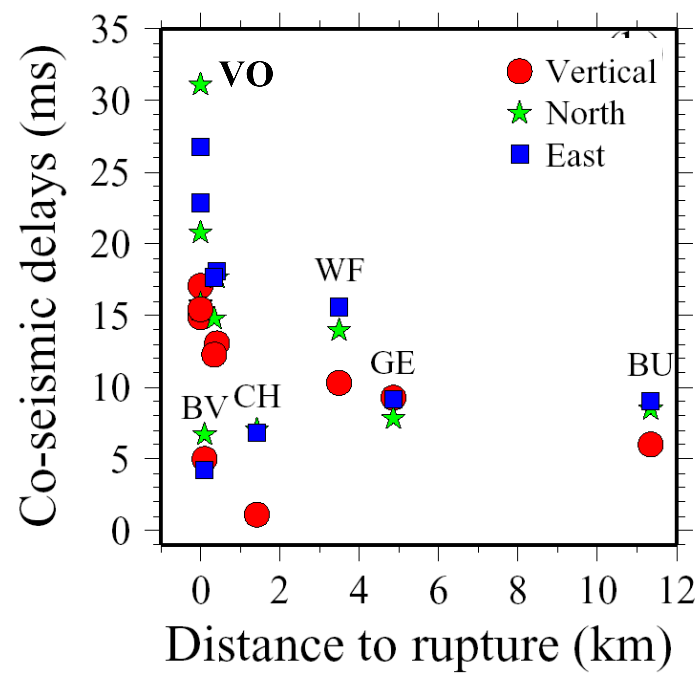

- The changes are strongest **(3% with Δt of minutes)** near the damaged FZ rock, but exist at all stations and do not change with source location (including depth).
- The effects reflect changes in the top damaged surface layer and shallow FZ damaged rock (e.g., 200-500 m)
- Similar results were obtained for earthquakes in California and Japan (e.g., Rubenstein & Beroza, 2004; Sawasaki et al., 2006; Nakata & Snieder, 211)).

Monitoring fault zone environments with correlations of earthquake waveforms (Roux and Ben-Zion, GJI, 2014)

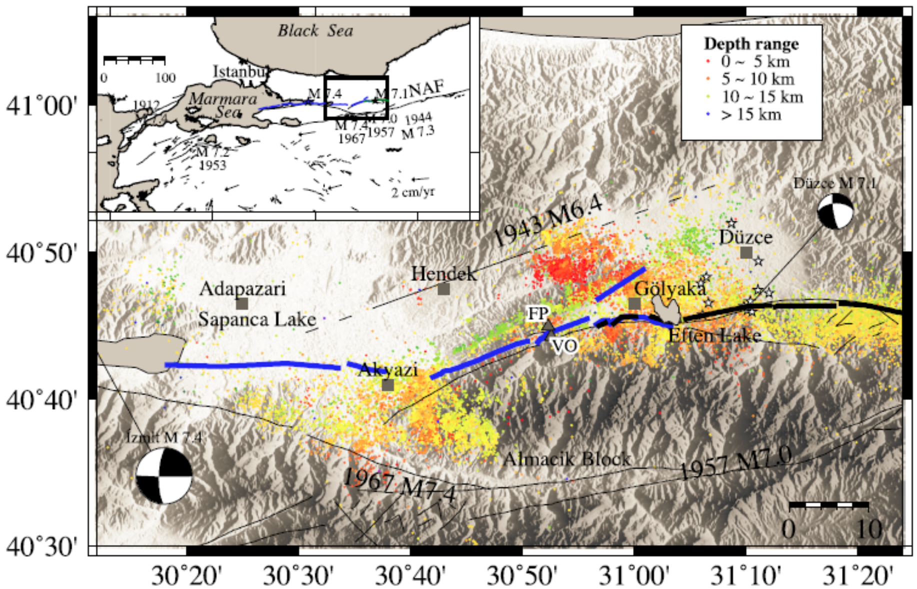

Aftershock waveforms allow using small time steps (min – hours) and high frequencies

Event properties

Power law size statistics
Magnitude range ~0-5 km
Depth range ~1-15 km
Evolving locations and rates

Seismograms of M2.8 event at stations VO and FP 400 m apart

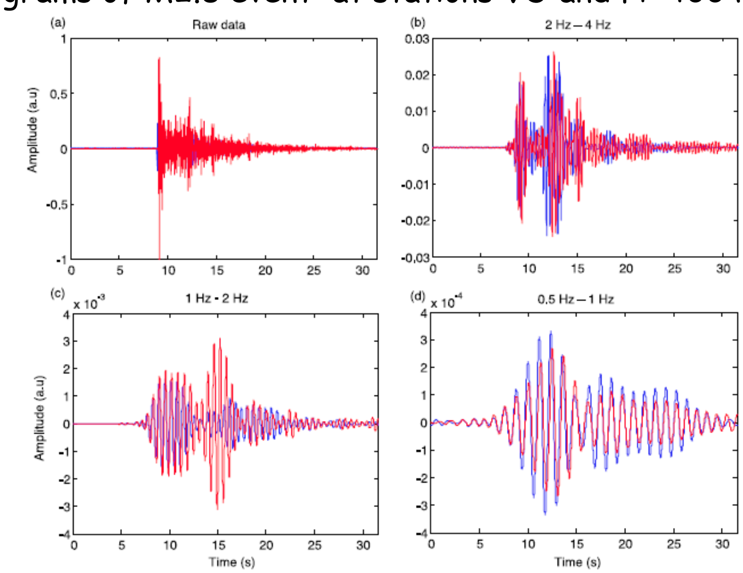

Processing

-filtering in frequency band of interest

-Calculating normalized cross correlations

$$C_{AB}(t) = \frac{\int_0^T S_A(\tau) S_B(t+\tau)\,d\tau}{\sqrt{\int_0^T S_A^2(\tau)\,d\tau \int_0^T S_B^2(\tau)\,d\tau}},$$

S_A, S_B are vertical component data at stations A and B

Coherence

Duzce →

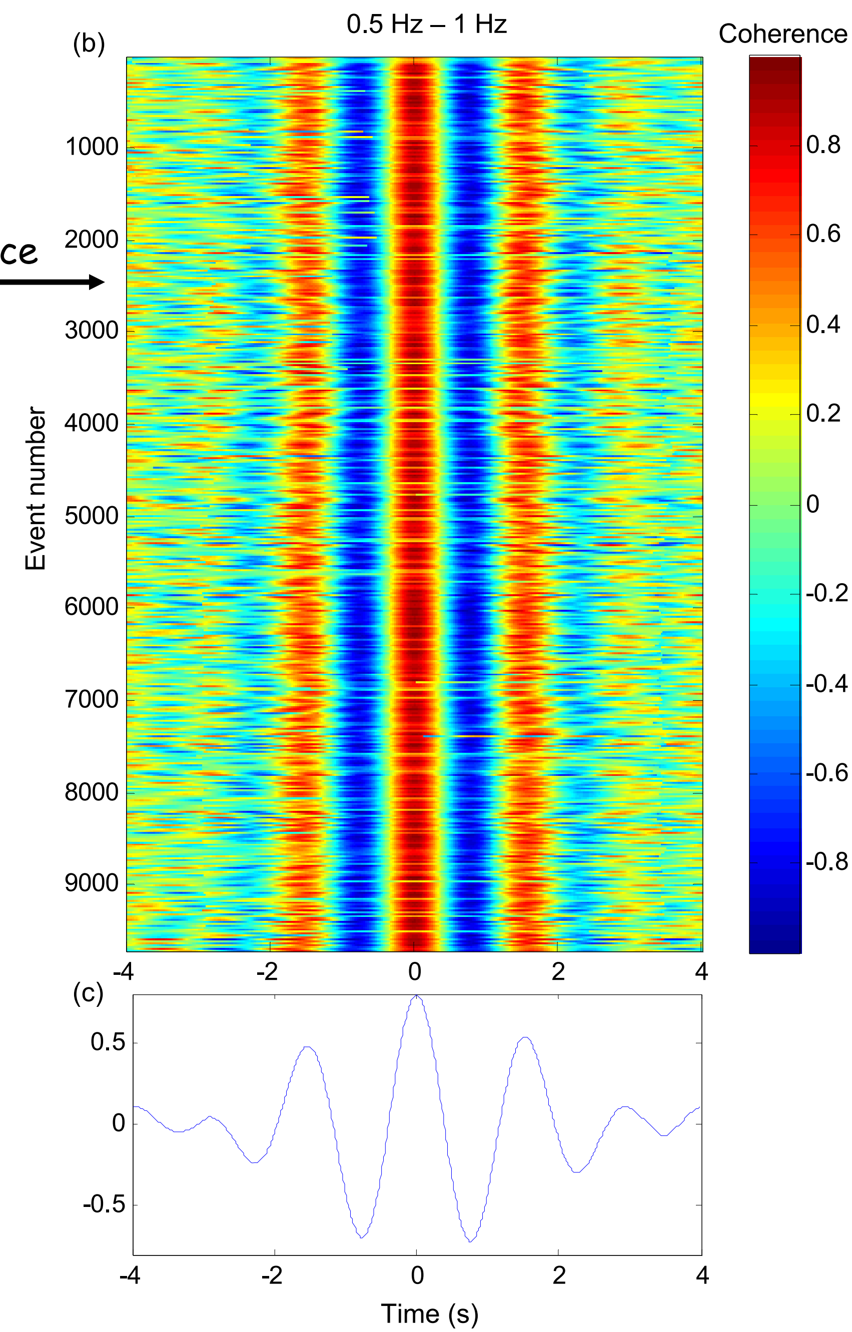

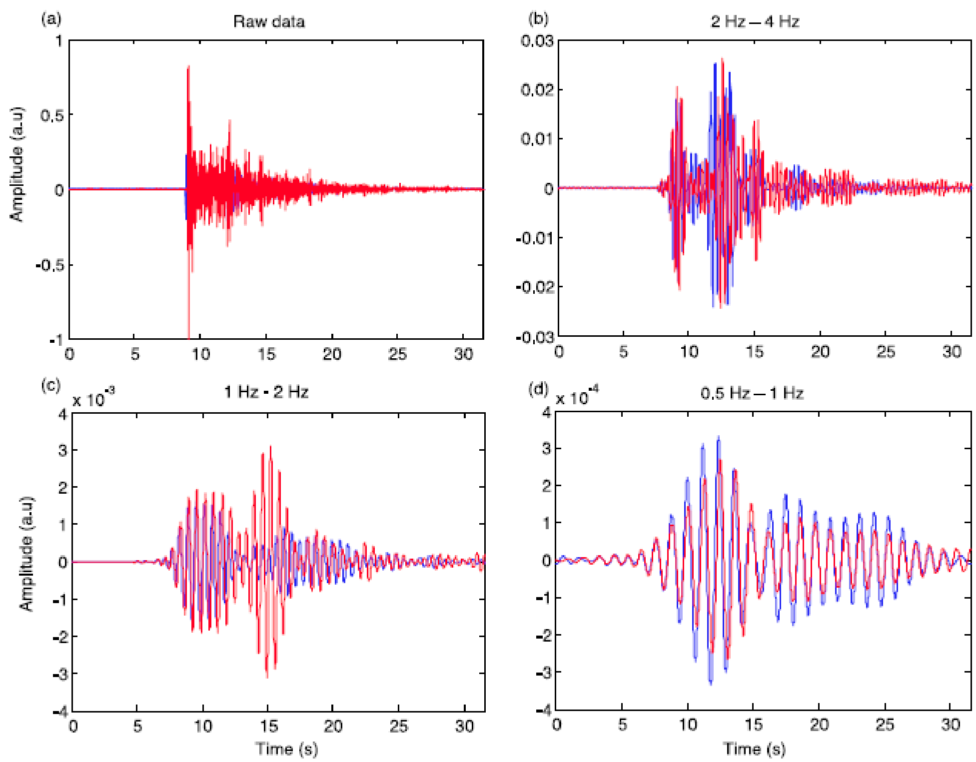

Seismograms of M2.8 event at stations VO and FP

Temporal evolution of correlation coefficient of different consecutive groups (overlapping) of events with the reference wavelet

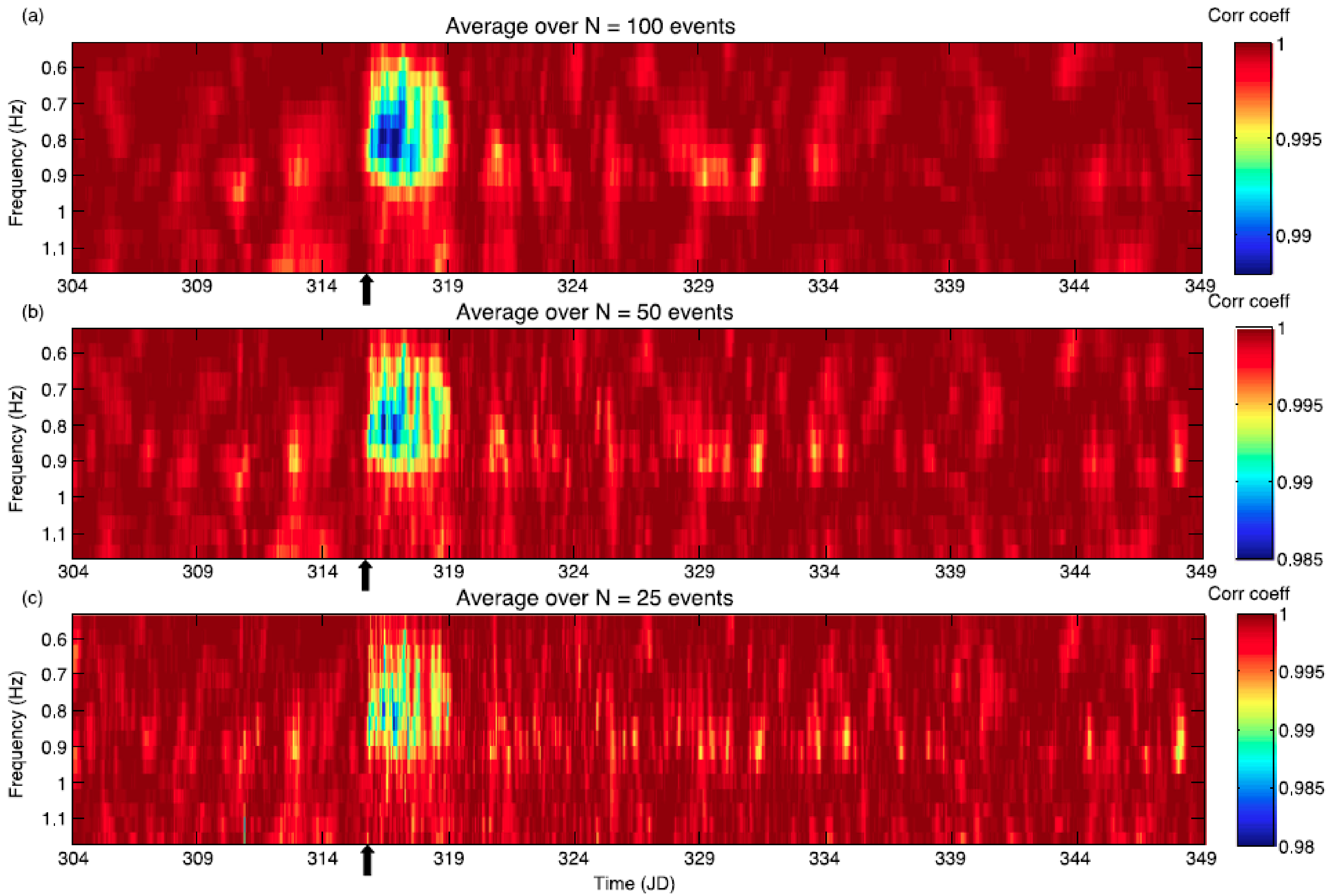

Temporal evolution of correlation coefficient of different groups of events with the referenece wavelet

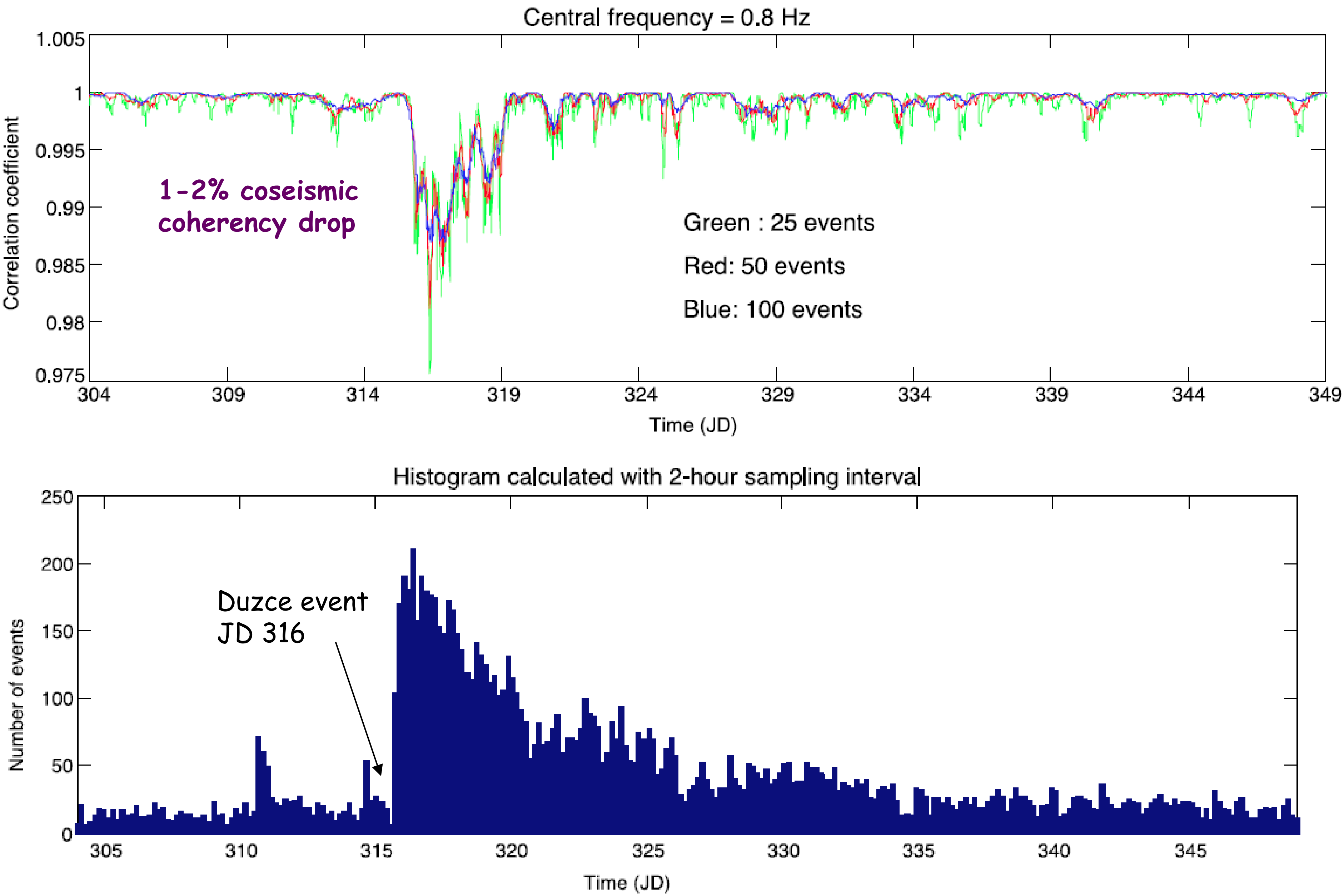

Temporal changes of fault zone site with spectral ratios

(Wu, Peng and Ben-Zion, GJI, 2009)

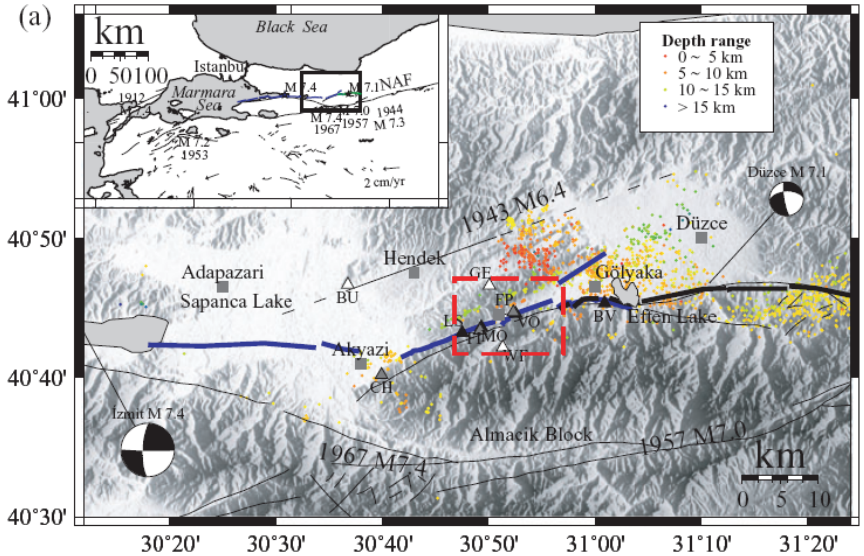

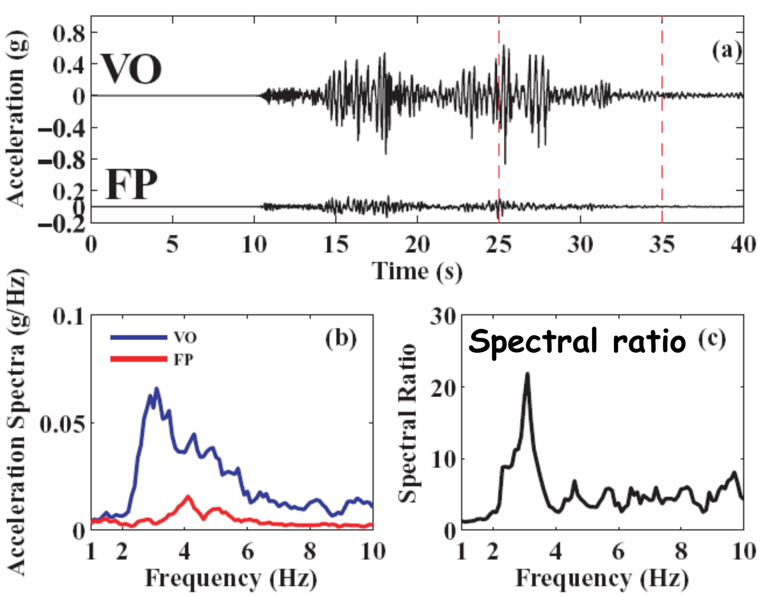

Spectral ratios of 15 events

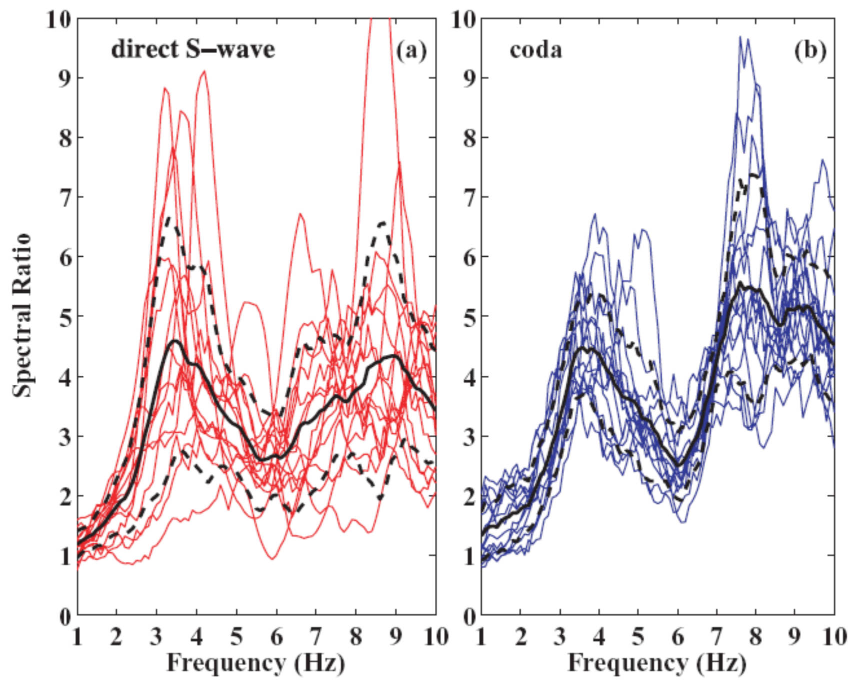

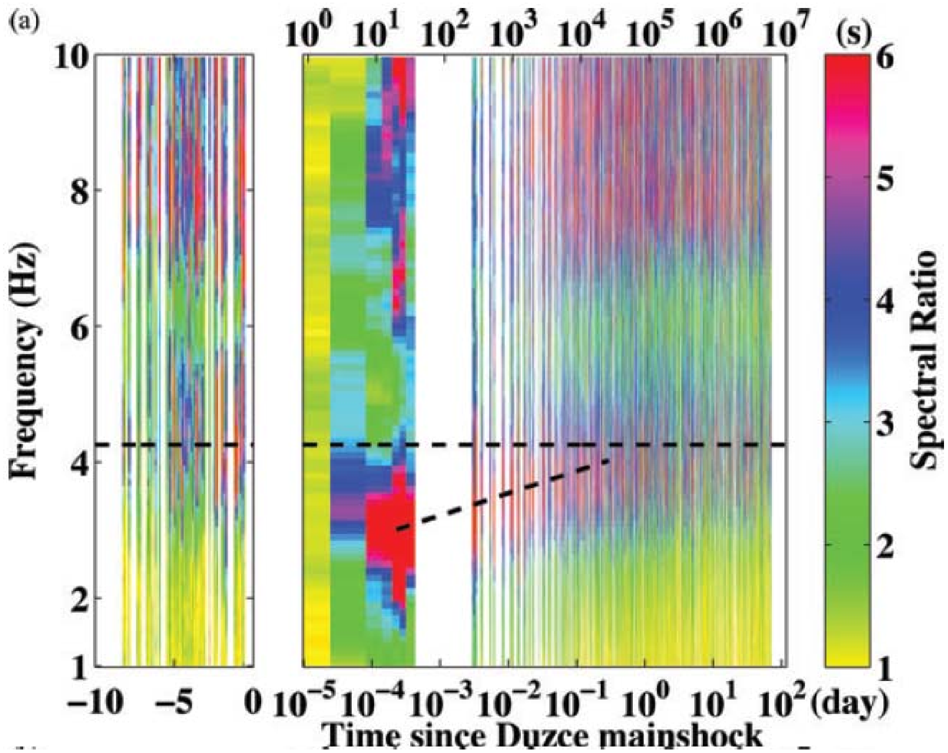

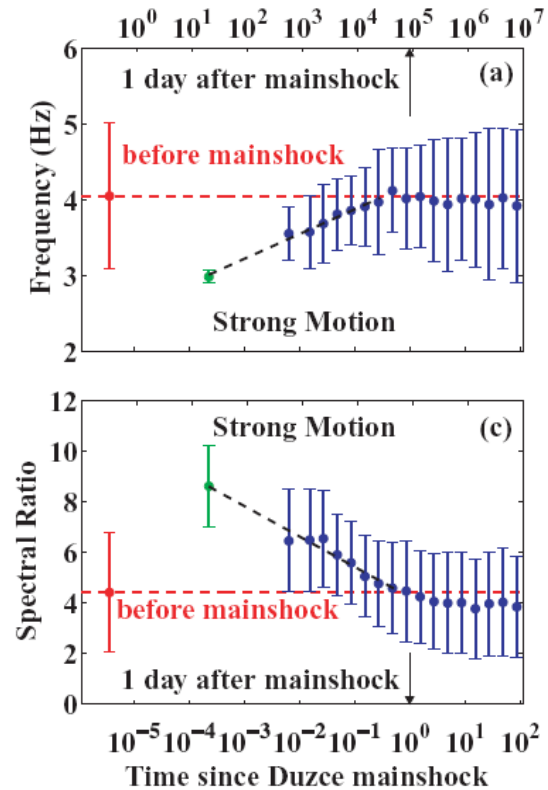

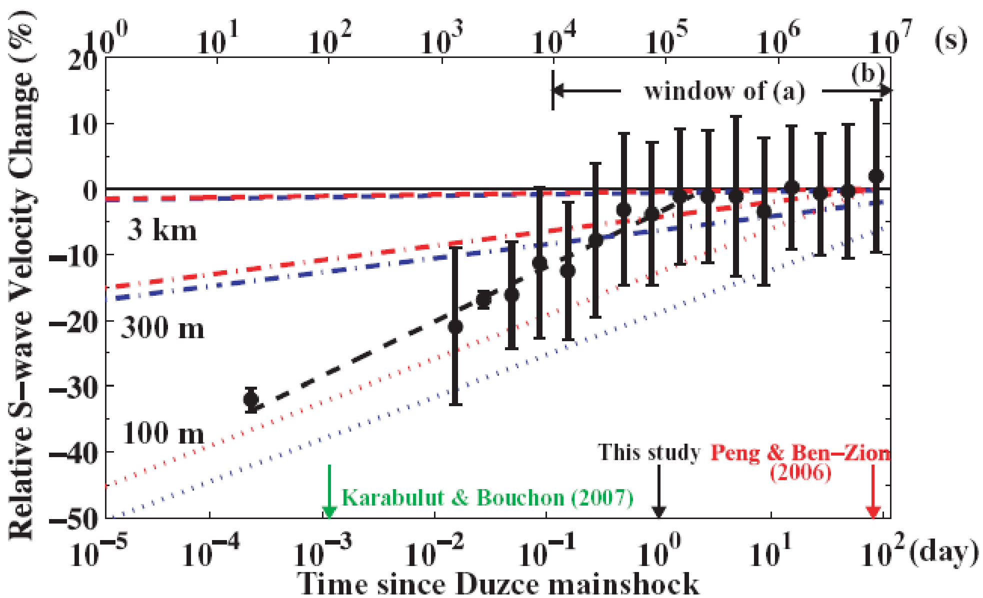

- The results suggest **>30% S velocity reduction in the top 100-300 m**, and logarithmic healing with strong effects over ~1 day (continuing with appreciable change over 3 months or longer duration).

- Similar results obtained by Karabulut and Bouchon (07), Rubenstein et al. (04, 05, 07), Sawazaki et al. (06, 08), and others for earthquakes in the US and Japan.

Temporal changes of seismic velocities after the M7.2 2010 El Mayor – Cucapah earthquake (Qin, Ben-Zion, Vernon, 2017)

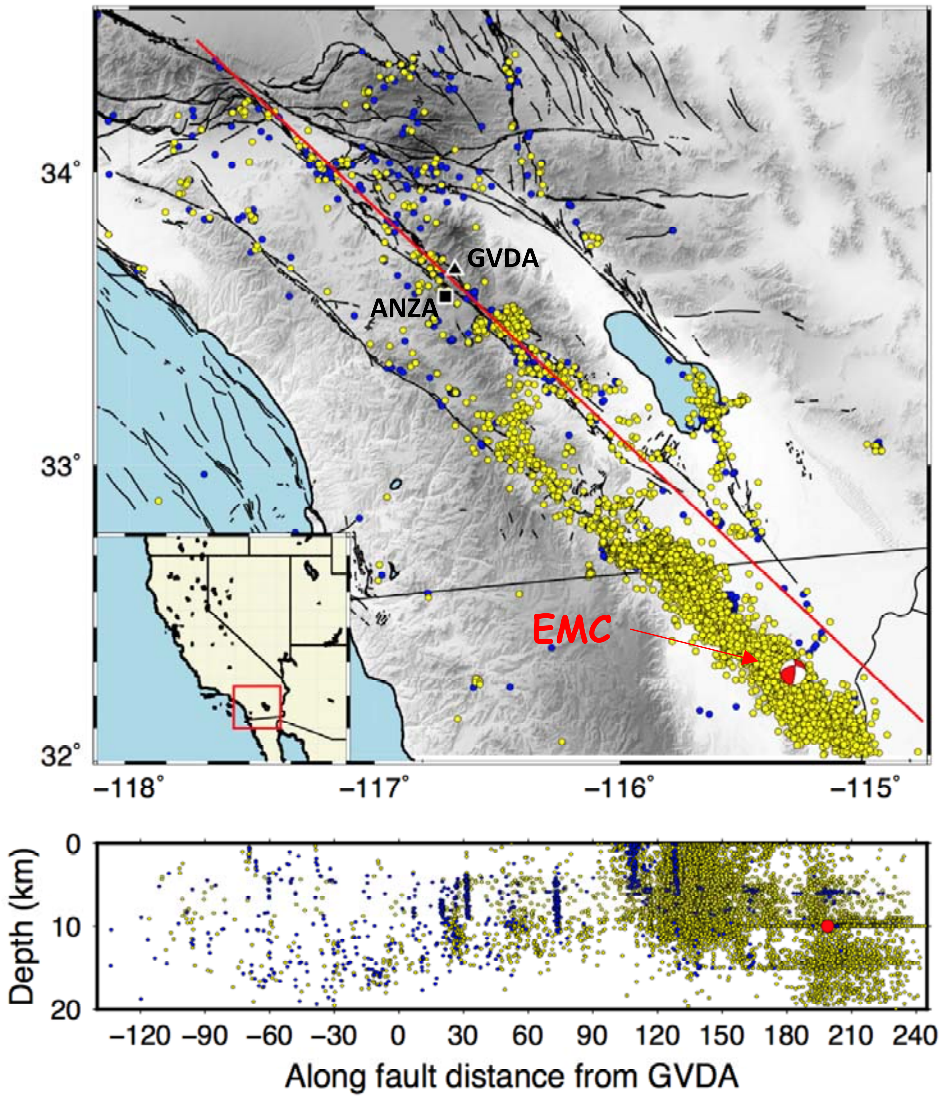

Blue: one month before EMC
Yellow: one month after

Garner Valley Downhole Array

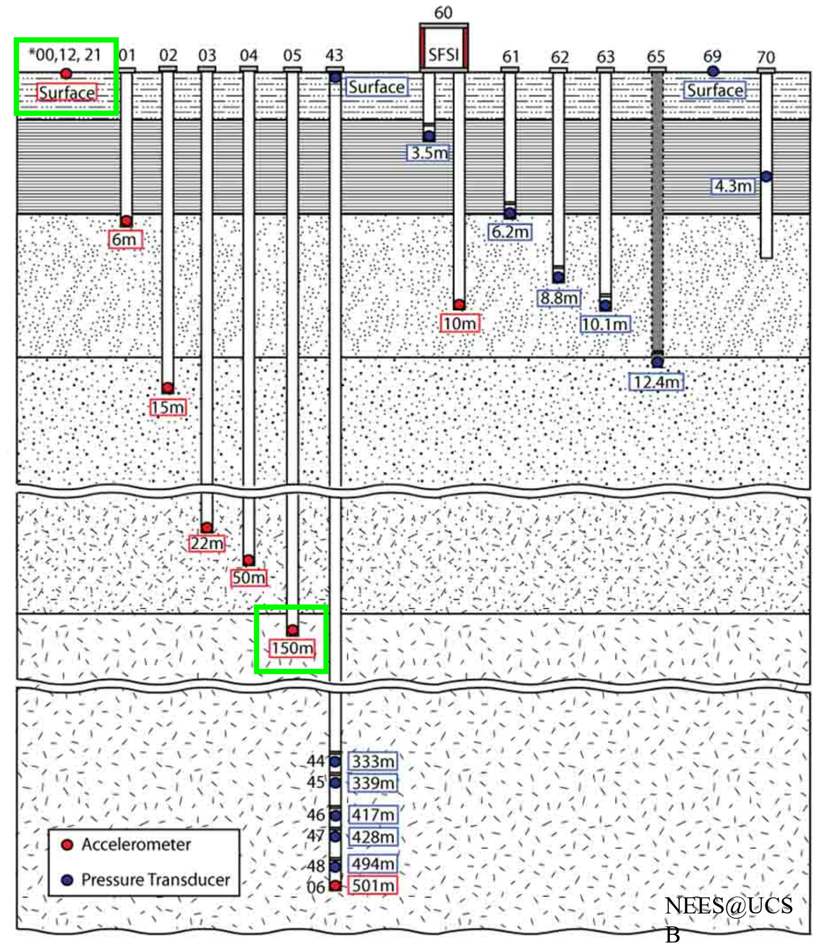

Use boreholes up to 150 m

Velocity analysis

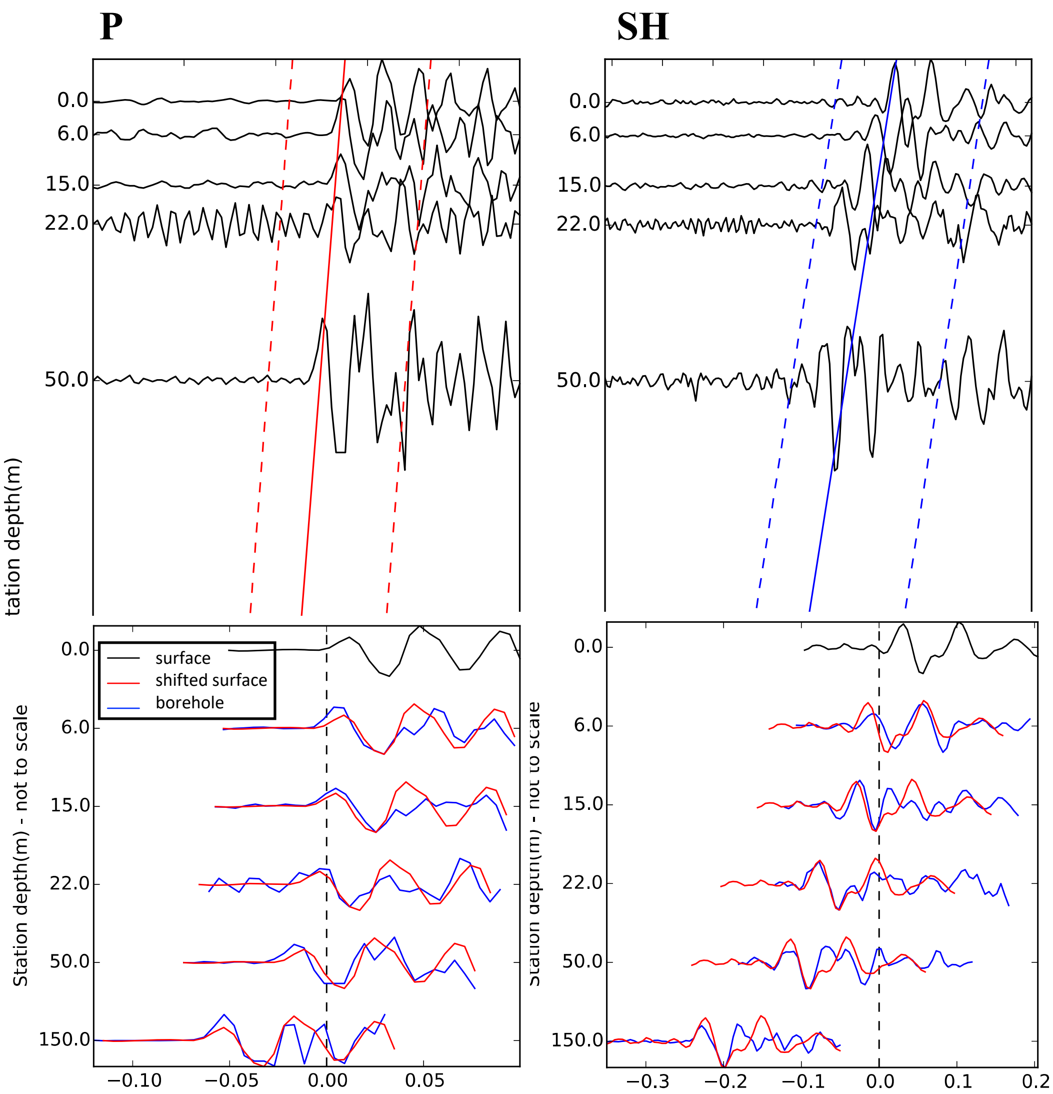

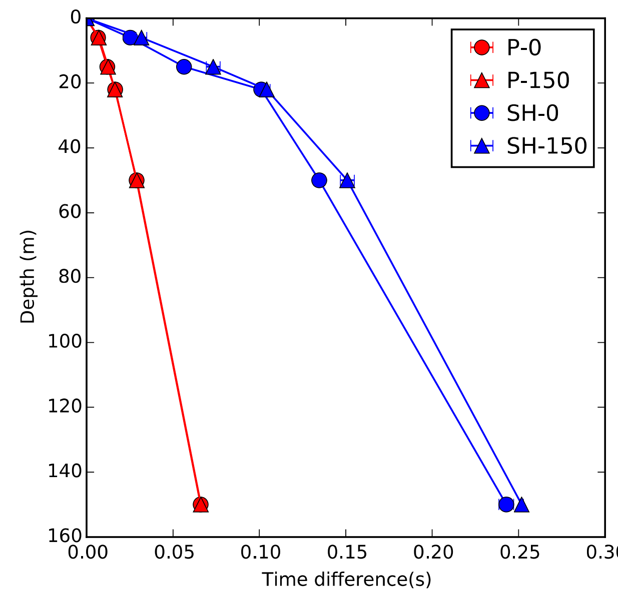

Station Depth (m)	Average Vp (m/s)	Average Vs (m/s)	Vp/Vs
6	1152	176	6.5
15	1328	213	6.2
22	1337	237	5.6
50	1724	350	4.9
150	2271	607	3.7

Note very low Vs and very large Vp/Vs ratios

Temporal changes

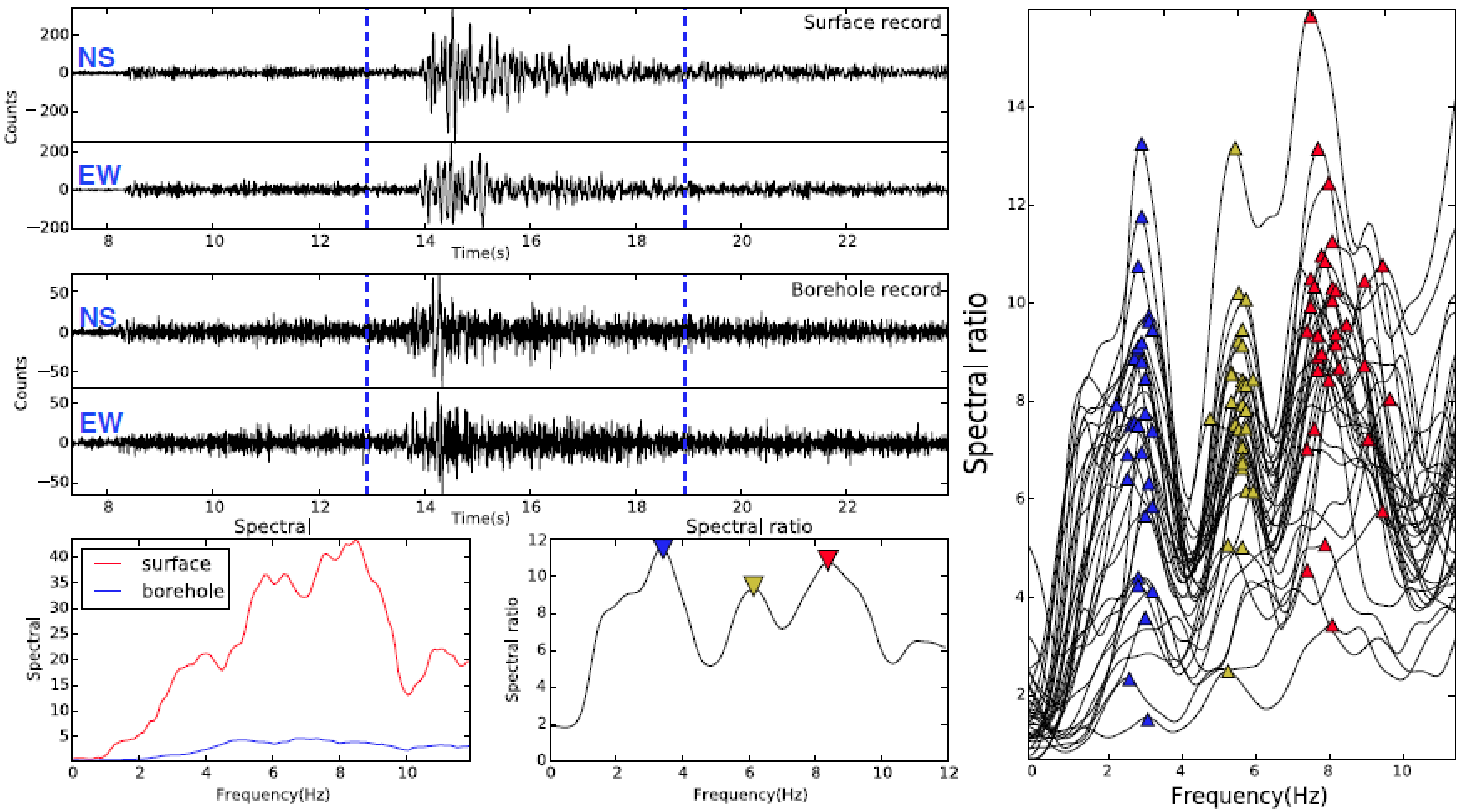

Temporal changes – S waves (two horizontal components)

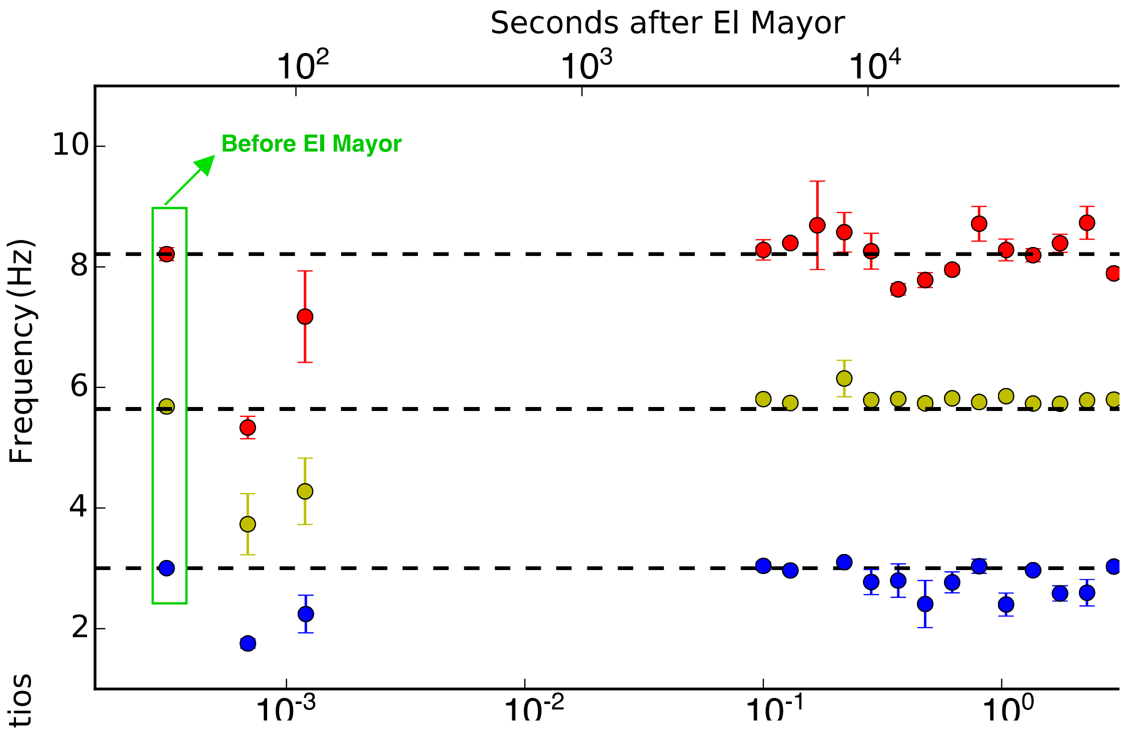

Temporal change of S wave velocity from two horizontal components

	Frequency peaks (Hz)	Average Vs (m/s)	Velocity drop
Before El Mayor	**3**	**600**	
	5.7	**684**	
	8.1	**694**	
After El Mayor	**1.8**	**360**	**40%**
	3.7	**444**	**35%**
	5.4	**463**	**33%**

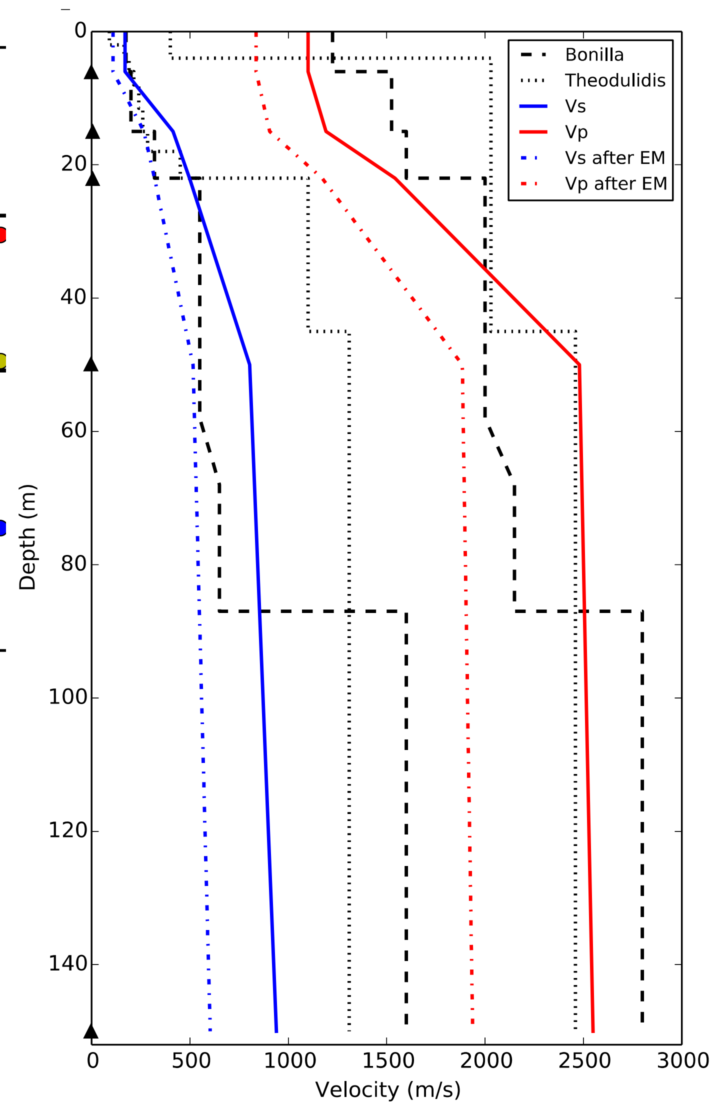

Very low velocities, high Vp/Vs ratios, large velocity changes in the very shallow crust

Implications for inferences at seismogenic depth?

Effects of shallow seismic properties on phase velocities up to 20 s

(Li, Niu and Ben-Zion, 2017)

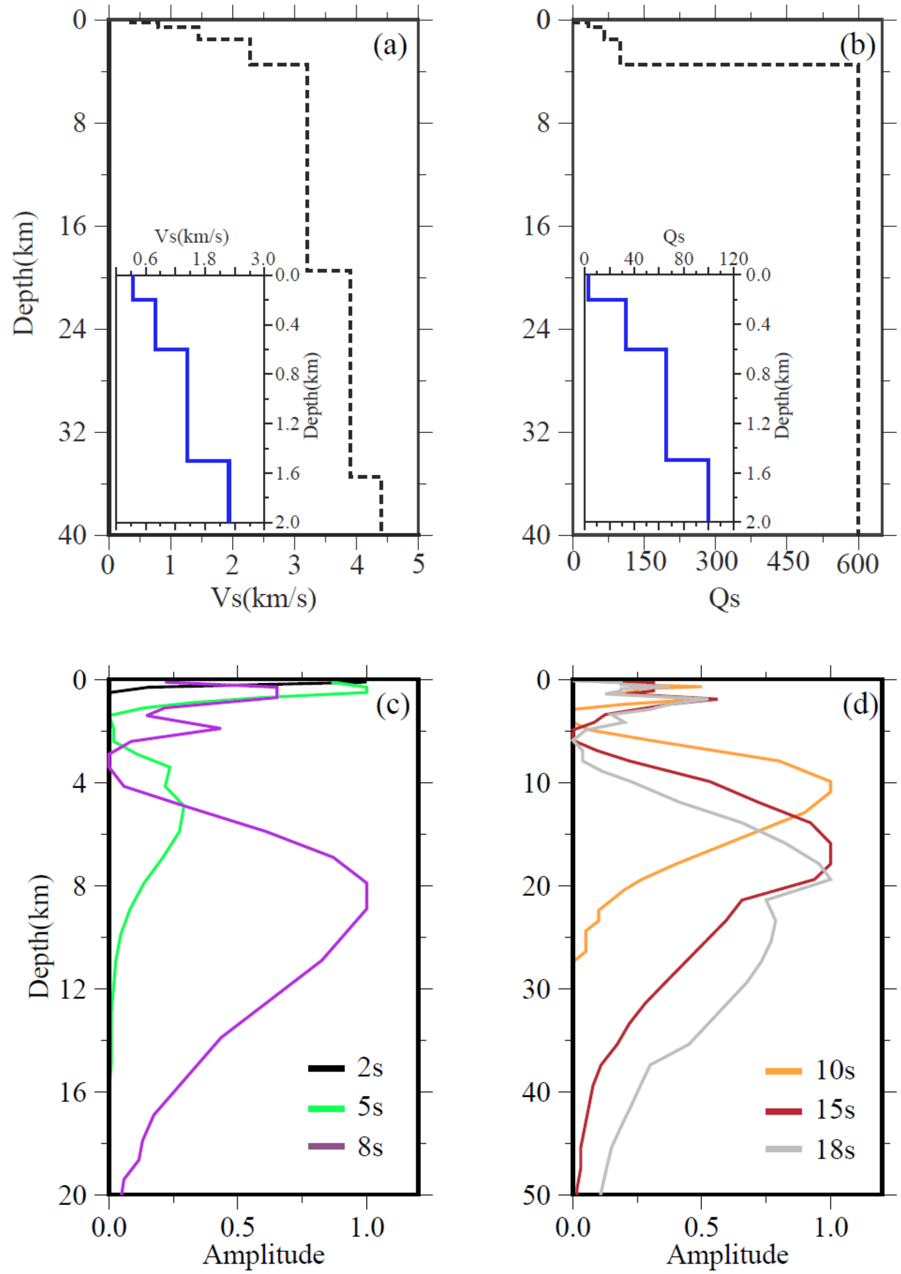

The low shallow velocities generate peak sensitivity at shallow depth up to 18 s (and beyond)

Case 1: 30% Vs drop in top 0.5 km

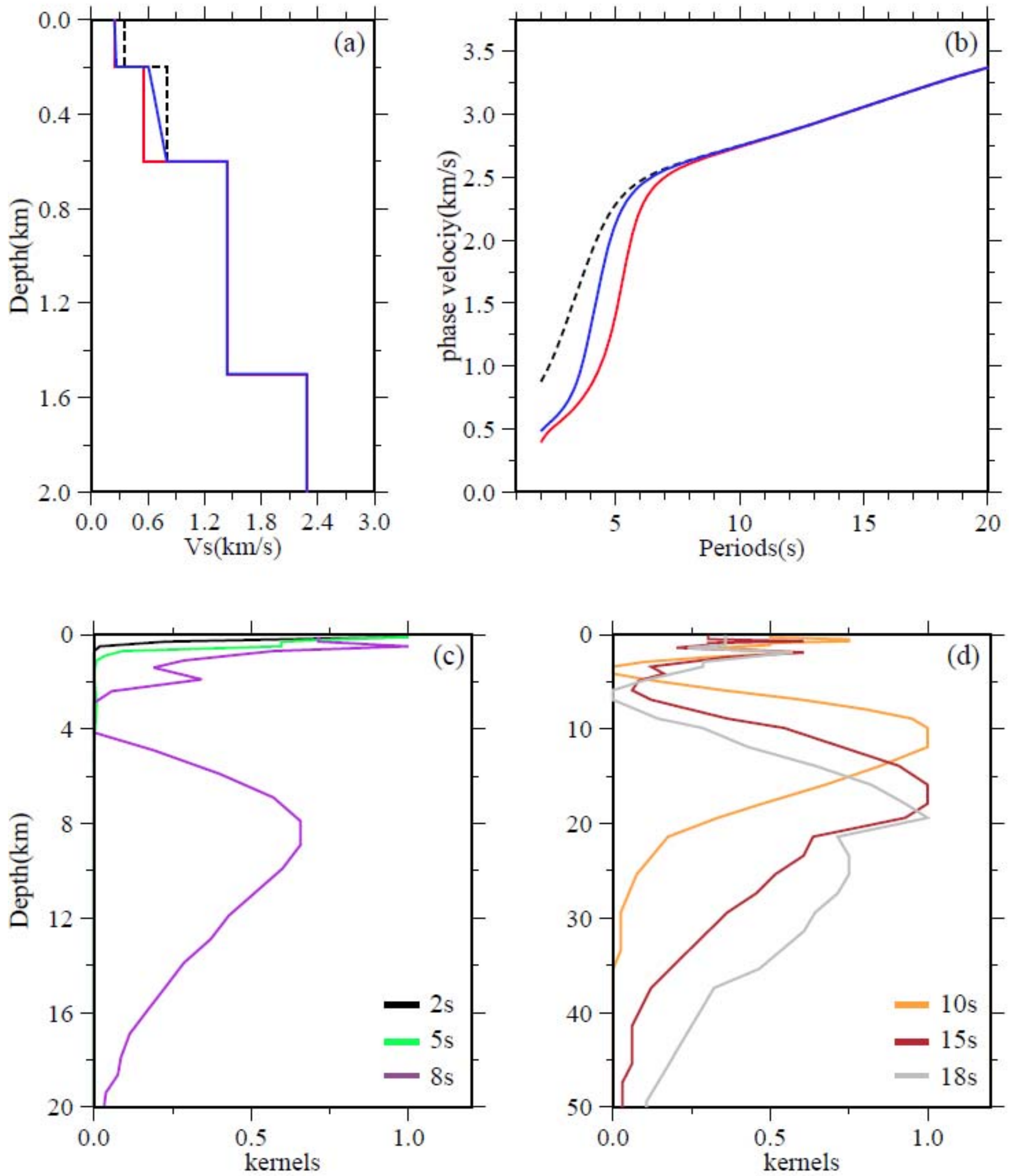

Note changes to phase velocities up to > 10 sec

Case 2: 30% Vs drop in top 1.5 km

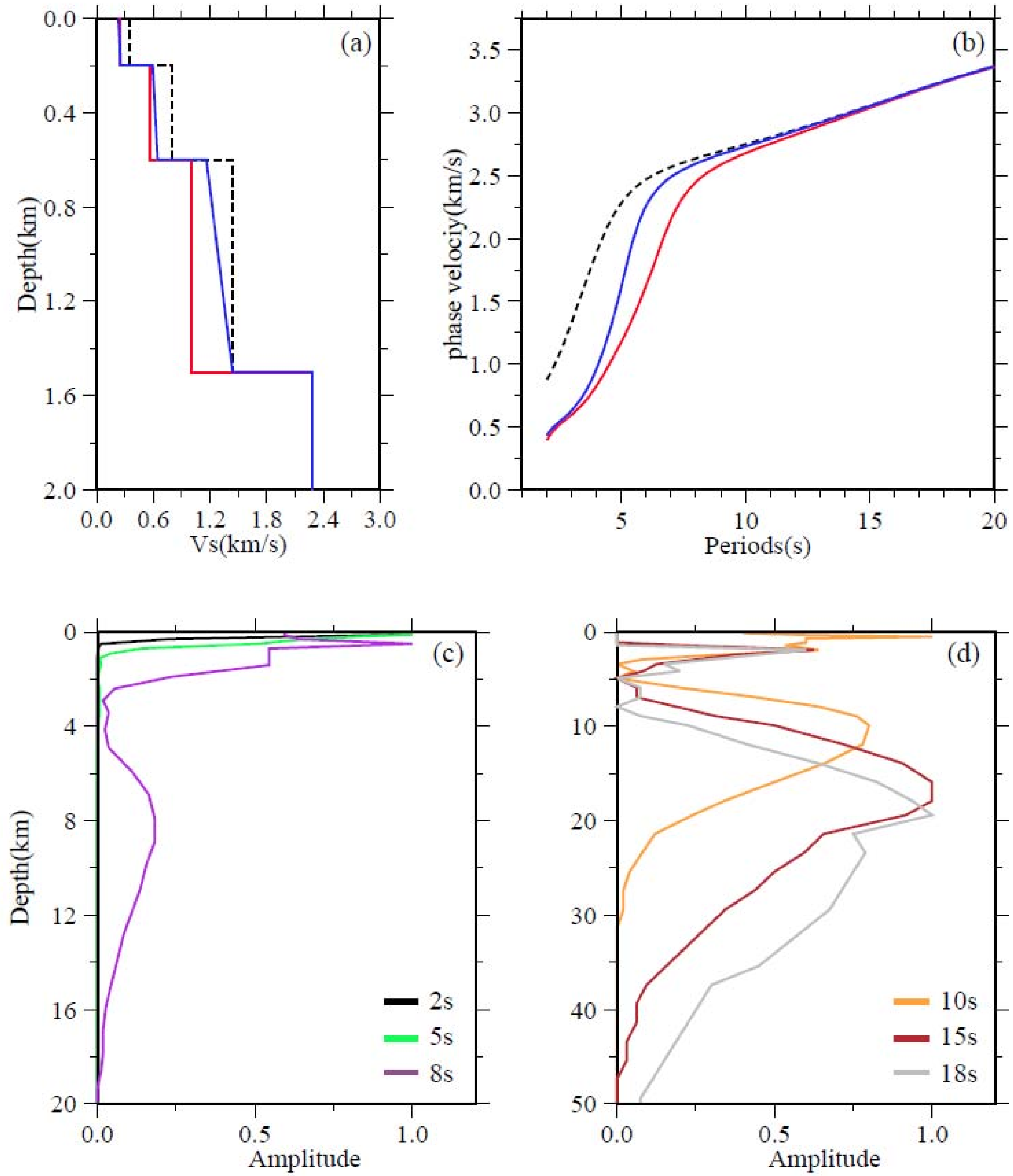

Note changes to phase velocities up to 20 sec

Case 1: 30% Vs drop in top 0.5 km

Case 2: 30% drop in top 1.5 km

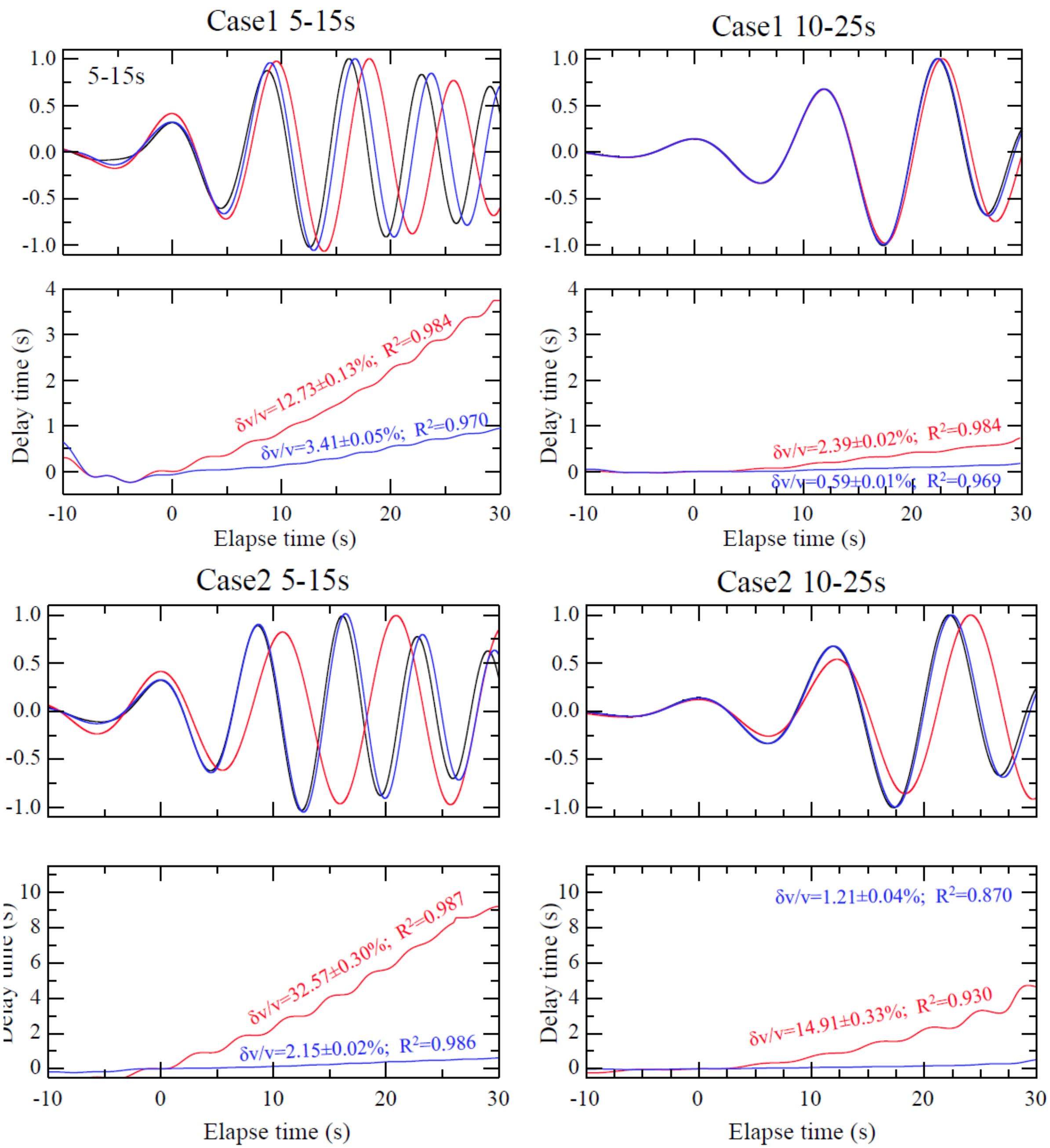

Need a strategy to separate these changes from changes at seismogenic depth!

Case 1: 30% Vs drop in top 0.5 km

Case 2: 30% drop in top 1.5 km

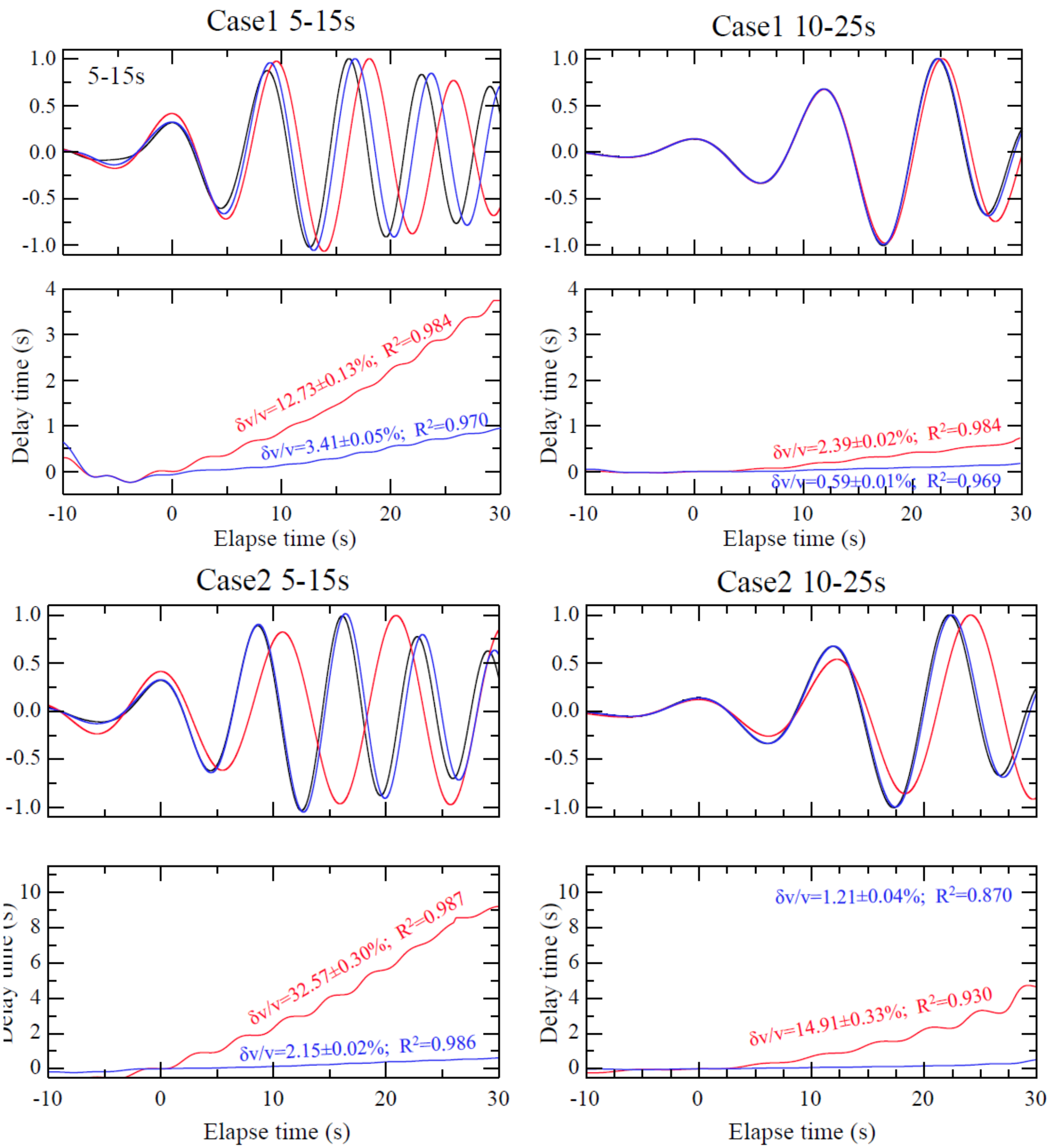

Similar values as reported changes at seismogenic depth!

In conclusion: the discussed techniques and array data allow us to resolve key structural elements of fault zone, temporal changes of properties and small earthquakes

Key references

Allam, A. A. and Y. Ben-Zion, 2012. Seismic velocity structures in the Southern California plate-boundary environment from double-difference tomography, *Geophys. J. Int.*, 190, 1181–1196, doi: 10.1111/j.1365-246X.2012.05544.x.

Ben-Zion, Y., F. L. Vernon, Y. Ozakin, D. Zigone, Z. E. Ross, H. Meng, M. White, J. Reyes, D. Hollis and M. Barklage, 2015. Basic data features and results from a spatially-dense seismic array on the San Jacinto fault zone, *Geophys. J. Int.*, **202**, 370–380, doi:10.1093/gji/ggv14.

Hillers, G., P. Roux, M. Campillo, Y. Ben-Zion, 2016. Focal spot imaging based on zero lag cross correlation amplitude fields: Application to dense array data at the San Jacinto fault zone, *J. Geophys. Res.*, 121, 8048-8067, doi: 10.1002/2016JB013014.

Meng, H. and Y. Ben-Zion, 2017. Detection of small earthquakes with dense array data: Example from the San Jacinto fault zone, southern California, *Geophys. J. Int.*, in review.

Qin, L., Y. Ben-Zion, H. Qiu, P.-E. Share, Z. E. Ross and F. L. Vernon, Internal structure of the San Jacinto fault zone in the trifurcation area southeast of Anza, California, from data of dense seismic arrays, *Geophys. J. Int.*, in review.

Qiu, H., Y. Ben-Zion, Z.E. Ross, P.-E. Share and F. L. Vernon, 2017. Internal structure of the San Jacinto fault zone at Jackass Flat from data recorded by a dense linear array, *GJI*, 209, 1369-1388.

Roux, P. and Y. Ben-Zion, 2014. Monitoring fault zone environments with correlations of earthquake waveforms, *Geophys. J. Int.*, **196**, 1073–1081, doi: 10.1093/gji/ggt441.

Roux, P., L. Moreau, A. Lecointre, G. Hillers, M. Campillo, Y. Ben-Zion, D. Zigone and F. Vernon, 2016. A methodological approach toward high-resolution surface wave imaging of the San Jacinto Fault Zone using ambient-noise recordings at a spatially dense array, *Geophys. J. Int.*, 206, 980–992.

Share, P.-E., Y. Ben-Zion, Z.E. Ross, Qiu, H and F. L. Vernon, 2017. Internal structure of the San Jacinto fault zone at Blackburn Saddle from seismic data of a dense linear array, *GJI*, doi: 10.1093/gji/ggx191. .

Zigone, D., Y. Ben-Zion, M. Campillo and P. Roux, 2015. Seismic Tomography of the Southern California plate boundary region from noise-based Rayleigh and Love Waves, *Pure Appl. Geophys.*, 172, 1007-1032.

Thank you